Comparative Proteomic Profiling of Receptor Kinase Signaling Reveals Key Trafficking Components Enforcing Plant Stomatal Development

Pengfei Bai[1,2], Minh Huy Vu[1,2], Chiaki Komatsu[1], Ophelia Papoulas[2], Kazuo Ebine[3,4,¶], Akira Nozawa[5], Tatsuya Sawasaki[5], Takashi Ueda[3,4], Edward M. Marcotte[2], Keiko U. Torii[1,2*]

[1] Howard Hughes Medical Institute, The University of Texas, Austin, TX 78712, USA
[2] Department of Molecular Biosciences, The University of Texas, Austin, TX 78712, USA
[3] Division of Cellular Dynamics, National Institute for Basic Biology, Okazaki, Aichi, 444-0867, Japan
[4] Basic Biology Program, Graduate Institute for Advanced Studies, SOKENDAI, Okazaki, Aichi, 444-0867, Japan
[5] ProteoScience Center, Ehime University, Matsuyama, Ehime, 790-8577, Japan

¶Present address: Graduate School of Science and Engineering, Saitama University, Saitama, 338-8570, Japan

Correspondence: Keiko U. Torii, ktorii@utexas.edu
* Lead Contact

Highlights:

- An atlas of ERECTA receptor kinase interactome and proximitome
- Proximity labeling identifies clathrin-associated proteins as ERECTA partners
- PICALM adaptors mediate both constitutive and ligand-induced ERECTA endocytosis
- Loss of *PICALM* impairs proper stomatal patterning

ABSTRACT

Receptor kinases are pivotal for growth, development, and environmental response of plants. Yet, their regulatory mechanisms and spatial dynamics are still underexplored. The ERECTA-family receptor kinases coordinate diverse developmental processes, including stomatal development. To understand the proteomic landscape of the ERECTA-mediated signaling pathways, we here report comparative analyses of the ERECTA interactome and proximitome by epitope-tagged affinity-purification (ET-AP) and TurboID-based proximity labeling (TbID-PL) mass-spectrometry, respectively. While ET-AP successfully recovered receptor complex components (e.g., TOO MANY MOUTHS), TbID-PL effectively captured transient associations with the components of endosomal trafficking, *i.e.* clathrin-mediated endocytosis (CME) machinery. We further identify that specific subfamily members of phosphatidylinositol-binding clathrin assembly proteins (PICALMs) interact with and synergistically regulate ERECTA internalization. Mutations of these *PICALMs* impair ERECTA endocytosis and lead to excessive stomatal clustering. Taken together, our work provides a proteomic atlas of the ERECTA signaling network and suggests that timely removal of receptor kinase by the endocytosis machinery is essential for active signal transduction enforcing stomatal patterning.

50 **INTRODUCTION**

51

52 Receptor kinases (RKs) constitute one of the largest gene families in plants, playing a
53 fundamental role in orchestrating growth, development, environmental response and immunity[1-6].
54 Among them, those with an extracellular leucine-rich repeat (LRR) domain comprise the largest
55 subgroups, with well-studied members including a phytohormone brassinosteroid receptor
56 BRASSINOSTEROID INSENSITIVE1 (BRI1)[7] and innate immunity receptor FLAGELLIN
57 SENSING2 (FLS2)[8]. The ERECTA family of three LRR-RKs, ERECTA (ER), ERECTA-LIKE1
58 (ERL1), and ERL2 regulate multiple aspects of developmental processes, including epidermal
59 patterning, organ morphogenesis, vascular differentiation, and meristem activity[9,10]. The
60 functional redundancy and synergy among these receptors are evident from the severe
61 developmental defects observed in *er erl1 erl2* triple mutants, which exhibit increased stomata
62 density and clustering, reduced plant stature and arrested inflorescence[11,12]. The pleiotropic
63 nature of ERECTA signaling is mediated by interactions with EPIDERMAL PATTERNING
64 FACTORs (EPFs) and EPF-LIKEs (EPFLs), a diverse family of endogenously secreted peptides
65 that enable spatiotemporal regulation of receptor signaling[13-16].

66

67 ERECTA fine-tunes stomatal development by balancing the proliferation and differentiation of
68 stomatal initial cells, meristemoid mother cells (MMCs), and dividing precursor cells called
69 meristemoids[12,17]. Studies in the past decade revealed the signal transduction pathways mediated
70 by ERECTA in a few developmental contexts[10]. Specifically, EPF2 is secreted from early stomatal-
71 lineage cells and binds to ERECTA to inhibit excessive stomatal formation. STOMAGEN/EPFL9
72 acts as an antagonistic peptide and competes with EPF2 for receptor binding, promoting stomatal
73 differentiation[15,18,19]. This ensures a tightly regulated developmental balance. ERECTA requires
74 its co-receptor TOO MANY MOUTHS (TMM) for selective ligand recognition[20-22]. Unlike ERECTA,
75 TMM lacks a cytoplasmic kinase domain and therefore does not directly participate in intracellular
76 signal transduction. Instead, ligand-activated ERECTA interacts with co-receptors, including
77 BRI1-ASSOCIATED KINASE1/SOMATIC EMBRYOGENESIS RECEPTOR KINASE3
78 (BAK1/SERK3) and related SERKs, which trans-phosphorylate and activate ERECTA[23,24].
79 Receptor-like cytoplasmic kinases (RLCKs), BRASSINOSTEROID-SIGNALING KINASE 1
80 (BSK1) and BSK2 also function downstream likely as a signaling scaffold that bridges ERECTA-
81 mediated signaling to the MAP kinase cascade via YODA[25].

82

83 The swift turnover of activated receptors involves multiple layers of control, with receptor
84 endocytosis playing a crucial role in modulating signaling intensity, duration, and spatial
85 distribution[26]. Plant RKs undergo both constitutive and ligand-induced endocytosis. For example,
86 it has been reported that BRI1 undergoes constitutive and ligand-induced endocytosis while
87 subcellular trafficking of ligand-activated BRI1-BAK1 complex has also been documented[27,28].
88 FLS2 undergoes rapid internalization upon ligand perception[29,30]. Accumulating evidence shows
89 that both BRI1 and FLS2 are internalized via clathrin-mediated endocytosis (CME)[28,31]. A recent
90 study demonstrated that one of the ERECTA-family members, ERL1, undergoes ligand-induced
91 endocytosis, and trafficking initially to multivesicular bodies (MVBs) and then to late endosomes
92 for vacuolar degradation. EPF1 peptide promotes TMM-dependent ERL1 internalization, whereas
93 STOMAGEN inhibits ERL1 endocytosis by retaining the receptor in the endoplasmic reticulum,
94 providing an additional layer of receptor regulation[32]. No specific components for ERL1
95 endocytosis are known. Given the functional overlap between ERL1 and ERECTA, it is plausible
96 that ERECTA undergoes similar endocytic regulation, although its intracellular trafficking
97 mechanisms remain poorly understood.
98
99 The interactome of LRR-RLKs has been extensively profiled, revealing an integrated network of
100 extracellular receptor-ligand interactions[33]. While proteomic studies have advanced our
101 understanding of RK signaling, its regulatory mechanisms and dynamic signaling processes still
102 remain a challenge. Conventional affinity purification-mass spectrometry has been instrumental
103 in identifying RK interactors[34,35]. However, it has inherent limitations in detecting transient or weak
104 interactions, leaving a significant portion of the RK intracellular network unresolved[36]. TurboID-
105 based proximity labeling (TbID-PL) has emerged as a powerful approach for mapping low-
106 abundant and transient interactors with high spatial and temporal resolution[37-40]. Here, we employ
107 a parallel proteomic approach using epitope-tagged affinity-purification (ET-AP) and TbID-PL
108 from the same biological samples to construct a comprehensive proteomic map of the ERECTA
109 signaling network. In addition to the canonical ERECTA signaling components, we identify a suite
110 of adaptor and accessory proteins linked to CME[41]. Among these, we discover that PICALMs, key
111 regulators of CME, associate with ERECTA and play a crucial role in receptor internalization and
112 homeostasis. Functional characterization of *picalm* mutants uncovers excessive stomatal
113 numbering and clustering, phenocopying higher-order *erecta* family loss-of-function mutants.
114 Collectively, our study establishes a proteomic atlas of the ERECTA signaling network and
115 highlights the significance of CME-mediated receptor dynamics in maintaining robust RLK
116 signaling and proper stomatal development.

117 **RESULTS**

118

119 **Comparative proteomic profiling of ERECTA-associated proteins**

120 To unravel the full proteomic landscape of ERECTA-mediated cellular receptor signaling, it is
121 imperative to simultaneously profile both the ERECTA-interacting proteome (*i.e.* those proteins
122 that tightly associate with ERECTA) and proximity proteomes (*i.e.* those proteins in the close
123 vicinity of ERECTA receptor complexes). To achieve this goal, we performed parallel epitope-
124 tagged affinity purification (ET-AP) and TurboID-based proximity labeling (TbID-PL) from the
125 same Arabidopsis seedling extracts (see Methods; Figure 1A). For this purpose, we generated a
126 transgenic Arabidopsis seedlings expressing *ERECTA-HA-TbID* fusion protein under the control
127 of the native ERECTA promoter in the *erecta* null allele, *er-105*. The expression of an ERECTA-
128 HA-TbID fusion protein fully rescued the characteristic inflorescence and stomatal patterning
129 defects of *er-105*, validating its biological functionality (Figure S1). Notably, immunoblot analysis
130 verified the efficient biotinylation of proximal proteins in TbID-PL experiments and the successful
131 isolation of the fusion protein (Figures 1B, S2).

132

133 Through the parallel proteomics approaches, we identified 715 proteins via TbID-PL and 278
134 proteins via ET-AP, with 50 proteins shared between the two approaches (Figure 1C, E, Table
135 S3). We first examined the proteomes specifically enriched by each approach. TbID-PL
136 prominently enriched transient and membrane-associated interactors, including proteins involved
137 in CME, most notably phosphatidylinositol-binding clathrin assembly protein (PICALM) family
138 members, the TPLATE complex, and dynamin-related protein (DRP) family proteins (Figure 1E).
139 On the other hand, ET-AP exclusively detected TOO MANY MOUTHS (TMM), a known regulator
140 of stomatal patterning that forms a stable receptor complex with ERECTA[22] (Figure 1E). It is
141 important to note that TMM is an LRR-RLP with an extracellular and transmembrane region but
142 lacking any recognizable cytoplasmic domain[42]. Since TbID was fused to the cytoplasmic domain
143 of ERECTA (Figure 1A), the absence of TMM biotinylation by ERECTA TbID-PL indicates that
144 the plasma membrane environment was preserved during labeling. Lastly, both approaches
145 effectively captured ERECTA itself, along with shared interactors like auxin efflux transporters
146 PIN3 and PIN7, hinting at a molecular link between ERECTA and auxin-mediated plant growth
147 control[43,44].

148

149 Consistent with our finding that TbID-PL preferentially captures dynamic and transient interactors
150 of the RK ERECTA, the identified proteins are significantly enriched in Gene Ontology (GO)

151 categories related to "protein targeting to membranes", "vesicle-mediated transport", and
152 "intracellular protein transport and endocytosis" (Figure 1F). Additional enriched categories
153 include "plant epidermis morphogenesis", "cell recognition", "cell division and cytokinesis", and
154 "ATP hydrolysis and biosynthesis", likely reflecting the broad range of biological processes
155 mediated by the ERECTA signaling. Subcellular localization analysis further revealed that
156 ERECTA-associated proteins are predominantly enriched at the plasma membrane and cytosol
157 (Figure 1D, Table S6), underscoring the spatial specificity of TbID-PL in detecting proximal
158 proteins. Together, these findings highlight the complementary strengths of TbID-PL and ET-AP
159 in defining the ERECTA-associated proteome. Specifically, our results indicate that TbID-PL
160 exhibits higher sensitivity in detecting transient and dynamic interactors, whereas ET-AP identifies
161 stable extracellular complexes, thereby providing a comprehensive view of ERECTA-associated
162 proteomic landscapes.
163
164 **Optimized TbID-PL enhances detection of ERECTA-signaling components and reveals**
165 **compartment-specific proteomic profiles**
166 Extensive genetic studies have identified the downstream components of ERECTA signal
167 transduction pathways[23,25,45-47]. However, we did not detect many such components through the
168 ET-AP and TbID-PL, possibly due to their low abundance. It is increasingly recognized that TbID-
169 PL in plants faces significant background noise owing to the endogenous biotin pools within plant
170 cells[48,49]. To improve the detection of biologically-relevant proximitome while minimizing
171 background noise, we optimized the labeling strategy by comparing the biotinylated proteomes of
172 ERECTA-HA-TbID seedlings treated with exogenous biotin (with biotin, 1hour) to a mock treated
173 control (without biotin, 1hour) (Figure 2A, Figure S2C; see Methods). This approach effectively
174 captured BAK1[23], the transient co-receptor of ERECTA as well as the downstream MAPKKK,
175 YODA[45] (Figure 2B, Table S4).
176
177 To enhance the membrane proximitome signals, we next performed microsomal fractionations,
178 which retained higher levels of full-length ERECTA with reduced biotinylation background signals
179 (Figure S2D). Through the ERECTA membrane TbID-PL, we are able to detect the membrane-
180 attached receptor-like cytoplasmic kinase BSK1, which likely relays the ERECTA signaling[25]
181 (Figure 2B, Table S5). We additionally detected the LRR-RK HAESA-LIKE1 (HSL1), which has
182 been shown to be expressed in stomatal-lineage cells and modulate stomatal development[50]
183 (Figure 2B). Notably, the endocytosis components PICALM4A and PICALM4B are robustly and
184 consistently detected in all four TbID-PL conditions. Additional consistent ERECTA TbID-PL

185 interactors include several RKs, TMK4[51], HERK1[52], LIK1[53], as well as ANGUSTIFOLIA, which is
186 a component of stomatal polarity complex[54], and the blue-light receptor PHOT1[55] (Figure 2C, D).
187 Together, our multilayered strategies of TbID-PL procedures effectively capture ERECTA
188 signaling components, enable detection of compartment-specific proximitomes, and establish the
189 core sets of proteins at the proximity of ERECTA that could guide future explorations.
190

191 **ERECTA interacts with the PICALM family of clathrin-mediated endocytosis (CME)**
192 **components**

193 Our ERECTA TbID-PL highlights the CME components as transient interactors of ERECTA. While
194 ERECTA-family RKs are known to undergo endocytosis, no specific components that recognize
195 ERECTA as a cargo have been identified[32,56,57]. To explore the subcellular regulatory dynamics
196 of ERECTA, we first analyzed its association with the CME machinery by constructing a
197 landscape of the ERECTA network using STRING database analysis[58] (see Methods). The
198 network grouped ERECTA-associated proteins into distinct functional categories: internalization
199 and protein trafficking, exocytosis, motor protein function, and stomatal development (Figure 2E).
200 Remarkably, none of the components other than the category of stomatal development have been
201 shown to directly interact with ERECTA, while they are overwhelmingly detected through TbID-
202 PL.
203

204 Among the newly identified ERECTA associatome, several CME-related components, notably
205 PICALM3, PICALM4A, and PICALM4B, captured our attention for their highly selective
206 enrichment (Figures 1-3). Importantly, PICALMs are known to function as adaptor proteins for
207 specific cargos but not required for general endocytosis[59]. To gain insight into their potential
208 relevance in stomatal development, we re-analyzed single-cell transcriptomic data[60] and found
209 that several PICALMs from Group 1 and Group 2 are differentially expressed across stomatal
210 lineage cells (Figure 3A, B). We therefore postulated that PICALMs may represent the yet
211 unidentified adaptors for ERECTA. To address this hypothesis, we first surveyed the protein-
212 protein interactions of ERECTA cytoplasmic domain (ERECTA-CD) and members of PICALM-
213 family throughout their five evolutionary subgroups[61] (Figure 3B), using *in vitro* translated proteins
214 in the Amplified Luminescent Proximity Homogeneous Assay Screen (AlphaScreen assay)[62]
215 (Figure 3C; See Methods). Indeed, we detected the highest interactions (*i.e.* normalized binding
216 activity) of ERECTA-CD with PICALM3 (Subgroup 1) and PICALM4A (Subgroup 2a) followed by
217 PICALM1A (Subgroup 1), consistent with their expression patterns in stomatal lineage cells.
218 Additionally, PICALM2A, 4B, 5A, and 6 exhibited positive but weaker interactions with ERECTA-

219 CD (Figure 3C). We further performed Co-immunoprecipitation (Co-IP) assays and demonstrated
220 that ERECTA indeed interacts with PICALM3, PICALM4A, and PICALM4B in Arabidopsis
221 protoplasts (Figure 3D). Combined, these findings establish PICALM family members of CME as
222 *in vivo* interactors of ERECTA, thereby implicating them in the endocytosis of ERECTA.
223
224 **PICALMs co-localize with ERECTA and regulate its endocytosis**
225 To elucidate the roles of PICALMs in ERECTA subcellular dynamics, we first examined co-
226 localization of ERECTA with PICALM proteins and endocytic markers in stomatal lineage cells.
227 Under mock conditions, ERECTA-YFP colocalized with both PICALM4A and *AtML1 promoter-*
228 *driven* RCI2A, a plasma membrane marker, across stomatal lineage cells (Figure 4A, B). Upon
229 treatment with Brefeldin A (BFA), which inhibits ADP-ribosylation factor guanine-nucleotide
230 exchange factor (ARF-GEF) activity and induces endosomal compartments (known as "BFA
231 bodies")[63], ERECTA-YFP accumulated within the BFA bodies in epidermal cells. Notably,
232 ERECTA-YFP co-accumulated with PICALM4A-RFP, but not with RCI2A, in BFA bodies, where
233 PICALM4A-RFP signals appear to encapsulate ERECTA-YFP, suggesting PICALM-mediated
234 recruitment of ERECTA into endosomal structures (Figure 4A, blue arrows; 4B; video 1).
235 ERECTA-YFP also partially colocalized with the trans-Golgi network (TGN) marker SYP43-RFP
236 and the early endosome marker ARA6-RFP at plasma membrane under mock conditions (Figure
237 4C). Following BFA treatment, ERECTA-YFP accumulated in endosomal compartments
238 containing these markers, indicating its trafficking through the TGN and early endosomal
239 pathways (Figure 4C). Additionally, ERECTA-YFP co-localized with the late endosome marker
240 ARA7-RFP under mock and wortmannin-treated conditions (Figure 4D), suggesting its
241 progression through late endosomal compartments. In contrast, its association with the vacuolar
242 membrane marker SYP22-RFP was limited (Figure 4D). These results demonstrate that PICALM-
243 mediated CME facilitates the dynamic trafficking of ERECTA-YFP from plasma membrane
244 through the TGN and early-to-late endosomal compartments.
245
246 To understand the role of PICALMs in ERECTA internalization, we assessed the formation of
247 ERECTA-YFP-positive BFA bodies in 'wild-type' (*ERECTApro::ERECTA-YFP in er-105*)
248 seedlings under BFA treatment (Figure 5A), compared with the *picalm1a;1b;4a;4b* higher-order
249 mutant background. In WT epidermal cells, ERECTA-YFP formed numerous BFA bodies,
250 particularly in stomatal lineage ground cells (SLGCs) and developing pavement cells (PCs),
251 suggesting elevated endocytic activity in these cell types (Figure 5A upper panel; 5B). Strikingly,
252 in the *pcalm1a; 1b; 4a; 4b* mutant background, the number of ERECTA-YFP-positive BFA bodies

253 is significantly reduced (Figure 5A lower panel, 5C), suggesting a marked impairment in ERECTA
254 internalization.
255
256 We next tested whether PICALMs are required for ligand-induced internalization of ERECTA. In
257 WT, treatment with exogenous mEPF2 peptide triggered cytoplasmic accumulation of ERECTA-
258 YFP puncta, overlapping with FM4-64, suggesting a ligand-activated endocytosis. This response
259 was largely reduced in *picalm* mutants, where ERECTA-YFP remained predominantly plasma
260 membrane-localized (Figure 5D, upper panel, 5E). Wortmannin (Wm) treatment induced
261 ERECTA-YFP accumulation in enlarged late endosomes (Wm bodies) in WT, and co-treatment
262 with mEPF2 + Wm further enhanced this effect. In contrast, *picalm* mutants showed minimal
263 ERECTA-YFP accumulation in Wm bodies under both conditions (Figure 5D, lower panel, 5F),
264 indicating impaired endocytic trafficking to late compartments. Together, these findings show that
265 PICALMs are required for both constitutive and ligand-induced endocytosis of ERECTA,
266 underscoring their role as cargo adaptors essential for receptor internalization and intracellular
267 trafficking.
268
269 ***PICALMs* redundantly enforce stomatal patterning by maintaining ERECTA homeostasis**
270 The association and co-localization of PICALM family members with ERECTA during CME
271 (Figures 1-4), together with impaired ERECTA internalization observed in *picalm* mutant (Figure
272 5), prompted us to investigate their functional roles in ERECTA-mediated stomatal development.
273 For this purpose, we first examined if the *picalm* mutants exhibit stomatal patterning defects.
274 Compared to wild type, *picalm* seedlings displayed escalating stomatal patterning defects,
275 characterized by increased stomatal number and clustering, with the higher-order mutant
276 (*picalm1a;1b;4a;4b*, *picalm1a;1b;3;4a;4b*) exhibiting a more severe phenotype than the single
277 (*picalm3*), double (*picalm1a;1b*, *picalm4a;4b*), or triple (*picalm3;4a;4b*) mutants (Figure 6A).
278 Importantly, the stomatal clustering phenotype resembles that of the *erecta*-family mutants[12]
279 (Figure S3). Quantitative analysis confirmed a significant increase in stomatal index and clustering
280 across multiple *picalm* mutants (Figure 6B, C), indicating that *PICALMs* are required for proper
281 stomatal patterning. To further explore the genetic relationship between PICALMs and ERECTA,
282 we generated a *picalm1a;1b;4a;4b;er-105* quintuple mutant and compared its phenotype to the
283 *erecta* null mutant, *er-105*. Both mutants exhibited comparable increases in stomatal and
284 meristemoid indices, with no significant additive effects in the quintuple mutant (Figure 6D, 6E).
285 This epistatic relationship suggests that PICALMs likely function within the ERECTA signaling
286 pathway, potentially facilitating its proper localization and functional complex formation.

287
288 To conceptualize this mechanism, we propose a model in which PICALMs, particularly PICALM4A,
289 4B, and PICALM3 act as cargo-specific adaptors that direct ERECTA into CME for proper
290 functional complex formation and signal transduction (Figure 6F). In *picalm* mutants, impaired
291 CME possibly causes ERECTA mislocalization or rerouting to noncanonical degradation
292 pathways, leading to disrupted signal transduction and abnormal stomatal development (Figure
293 6G).
294
295
296 **DISCUSSION**
297
298 In this study we comprehensively mapped the ERECTA signaling network in Arabidopsis using a
299 dual proteomic strategy, ET-AP and TbID-PL. Our findings not only recovered stable ERECTA
300 receptor complex components but also identified a dynamic cohort of transient, low-abundance
301 interactors, notably CME components such as PICALMs. Functional characterization of PICALMs
302 demonstrates their essential role in ERECTA internalization and protein homeostasis, with higher-
303 order *picalm* mutants phenocopying the excessive stomatal number and clustering observed in
304 *ERECTA*-family loss-of-function mutants. A previous study has demonstrated ligand-induced
305 endocytosis of the ERECTA-family member, ERL1[32], however, the specific adaptors facilitating
306 this process remained unknown. Our work identifies the components of CME that recognize
307 ERECTA as a cargo and further emphasizes that CME-mediated receptor dynamics are
308 indispensable for ERECTA receptor kinase-mediated stomatal patterning (Figure 6).
309
310 While proteomic profiling has been increasingly utilized to uncover receptor kinase interactors[64,65],
311 many challenges still persist that hamper the identification of low-abundance or transient
312 interactors without disrupting the native protein complex in the membrane environment. Our
313 optimized, combinatorial approach using ET-AP and TbID-PL enabled the detection of both
314 known components of the ERECTA signal transduction pathways as well as previously
315 undetected components. Technically, the exclusive detection of TMM by ET-AP, but not by TbID-
316 PL (Figure 1) highlights the preservation of the native plasma membrane environment during
317 proximity labeling, ensuring the reliability of our *in vivo* proteomic data. Our refined TbID-PL
318 enriched low-abundance signaling components like BSK1 and YODA (Figure 2), which are
319 otherwise difficult to detect using conventional methods. ERECTA regulates diverse roles in
320 development and environmental response[9,66], and as such, the identification of additional

321 interactors not previously associated with the ERECTA pathways, such as LIK1 and TMK4
322 (Figures 1, 2), may pave a path for future investigations of signal crosstalk.
323
324 The exclusive identification of CME components by TbID-PL highlights the transient nature of
325 their interactions with the receptor kinase (Figure 1). For example, the PICALM members,
326 PICALM1A, PICALM3, and PICALM4s, associate with ERECTA to varying degrees, and exhibit
327 unequal redundancy in enforcing stomatal patterning (Figure 6A-C). Unlike metazoan
328 counterparts, which comprise only four members in humans, the PICALM family is vastly
329 expanded in plants, with 18 members in Arabidopsis[67]. These AtPICALMs contain a conserved
330 ANTH (AP180 N-terminal homology) domain, which is essential for binding to phosphatidylinositol
331 lipids and clathrin, facilitating cargo endocytosis[67]. However, their slight structural differences may
332 enable them to interact with the same cargo with different affinity, as we observed for ERECTA
333 (Figure 3C), and/or alternatively, with distinct sets of membrane cargos or adaptor proteins. In
334 fact, a recent study suggests that PICALM1A and PICALM1B interact with R-SNAREs and clathrin
335 at the plasma membrane, where they regulate R-SNARE recycling to support plant growth[59].
336 Additionally, PICALM5A and PICALM5B are required for CME during pollen tube elongation by
337 maintaining tip localization of ANXUR, a receptor kinase sensing cell wall integrity[68]. PICALM4A
338 (also known as ECA4) has also been shown to act synergistically with other clathrin adaptor
339 protein EPSIN to support apical cell growth in pollen tubes[69]. Moreover, PICALM4A/ECA4 has
340 been implicated in the endocytosis of both the brassinosteroid receptor BRI1 and the ABA
341 exporter ABCG25 in roots[70]. In addition to stomatal patterning defects, we observed that higher-
342 order *picalm* mutations confer broader developmental defects, including reduced fertility and
343 impaired root elongation (Figure S5). Therefore, these PICALM subfamily members identified
344 through TbID-PL likely regulate additional clients beyond ERECTA.
345
346 We observed cell-type specific differences in ERECTA internalization across the epidermis, with
347 notably high internalization activity in developing stomatal lineage ground cells (SLGCs) and
348 pavement cells, and low levels in meristemoids (including MMCs) and GMCs (Figure 5A-B, 5D-
349 E). It is well established that ERECTA perceives EPF2 and restricts the initiation of stomatal cell
350 lineages via MAP Kinase-mediated degradation of SPCH proteins[16,17,19,71,72]. High activity of
351 ERECTA internalization in the SLGCs and pavement cells suggests that ERECTA signaling is
352 actively restraining their division potential, therefore limiting their re-entry into stomatal cell
353 lineages. This view is supported by the recent report that SPCH protein levels determine whether
354 SLGCs undergo asymmetric division or differentiate into mature pavement cells, a decision

355 impacted by EPF-signaling neighboring cells[73]. The EPF-ERECTA-family ligand-receptor system
356 is known to function in both autocrine and juxtacrine signaling[74,75]. How PICALMs-mediated
357 endocytosis influences these distinct modes of peptide-receptor signaling is an interesting future
358 question. We also observed that while ERECTA co-localized with PICALM4A at the plasma
359 membrane in stomatal lineage cells, it was notably absent from the cell plates of dividing guard
360 mother cells (GMCs) (Figure 3C). In contrast, another ERECTA-family receptor, ERL1, was
361 present at the cell plates and co-localized with PICALM4A in these dividing cells (Figure S7). This
362 spatial divergence suggests that PICALM4A may differentially associate with ERECTA-family
363 members depending on subcellular context or developmental stage. Notably, the enhanced
364 stomatal clustering phenotype observed in the *picalm1a;1b;4a;4b;er-105* combination mutant,
365 compared to *er-105* alone, further supports the notion that PICALMs may mediate trafficking of
366 multiple ERECTA-family receptor kinases.
367
368 During the EPF ligand recognition by ERECTA family receptors, the EPF1/2 antagonist
369 Stomagen/EPFL9 triggers stalling of ERL1 in the endoplasmic reticulum, likely owing to
370 dysregulated receptor retrieval from the plasma membrane[32]. The process likely involves the
371 endoplasmic reticulum-resident chaperone complex SDF2-ERdj3B-BiP, which facilitates proper
372 translocation of ERECTA-family RKs from the endoplasmic reticulum to plasma membrane[76,77].
373 In the epidermis of WT seedling, we occasionally observed ERECTA localized to endoplasmic
374 reticulum in addition to plasma membrane (Figure S6), suggesting the timely retrieval of ERECTA
375 via a specific internalization pathway may serve as a regulatory checkpoint to maintain receptor
376 homeostasis and proper signaling output.
377
378 Our observations also imply that the subcellular dynamics of ERECTA may be coupled with its
379 post-translationally modifications. Specifically, EPF2-induced activation of ERECTA triggers its
380 phosphorylation by coreceptor BAK1, followed by ubiquitination via the U-box E3 ligases PUB30
381 and PUB31, to attenuate signaling[24]. This process likely promotes to ubiquitination-dependent
382 internalization of ERECTA, consistent with prior findings that ubiquitination promotes BRI1
383 endocytosis and enables its recognition at the trans-Golgi network/early endosomes (TGN/EE)
384 for vacuolar targeting[78]. Consistently, a very recent study identified specific ubiquitination sites of
385 ERECTA and further demonstrated that ligand-activated ubiquitination triggers the endocytosis of
386 ERECTA[79]. In that study, the high accumulation of ubiquitination-deficient mutant version of
387 ERECTA at the plasma membrane conferred the inhibition of stomatal development, indicative of
388 the overly activated ERECTA signaling due to failed attenuation. In contrast, we here revealed

389 that the loss-of-function mutations of *PICALM* sub-family members perturbs the endocytosis of
390 ERECTA and result in stomatal clustering (Figures 5, 6), indicating that ERECTA signaling
391 pathway is defective in the absence of *PICALMs*. This apparent paradox, whereby defective
392 endocytosis of ERECTA lead to opposite signaling outcomes, raises interesting question about
393 the multiple layers of regulation imposed by receptor trafficking. We speculate that the activation
394 of ERECTA receptor complex requires the formation of membrane subdomains reinforced by the
395 PICALM mediated cargo sorting and vesicle formation. In such a case, PICALMs may facilitate
396 the assembly of signaling-competent receptor-coreceptor complexes within specific plasma
397 membrane nanodomains. Alternatively, this early activation process can be mechanistically
398 distinct from the later step of ubiquitination-mediated internalization and eventual degradation of
399 ERECTA that attenuate signaling. It is likely that different endocytic routes downstream of
400 PICALMs versus ubiquitination direct ERECTA toward distinct subcellular fates. Additionally,
401 PICALMs may generally facilitate endocytic trafficing, and if so the *picalm* higher-order mutants
402 could disrupt additional factors that impact ERECTA signaling as well as stomatal development.
403
404 These findings collectively support the model that ERECTA signal output is not solely dictated by
405 receptor abundance, but rather by its dynamic partitioning into specialized membrane domains
406 and intracellular compartments. Further understanding of ERECTA receptor trafficking provides
407 a foundation for future research into how membrane dynamics shape cellular differentiation and
408 patterning. Looking forward, our proteomic atlas provides an example for dissecting other RLK
409 networks, particularly those governing environmental responses where trafficking may modulate
410 signaling plasticity.
411
412
413 **Limitations of the study**
414 Due to technical reasons, our TbID-PL approaches lack ligand-induced proteomic profiling with
415 exogenously synthesized EPFs, making it challenging to distinguish receptor dynamics before
416 and after ligand perception. However, under native conditions we used, plant cells endogenously
417 secreted EPF peptides, leading to continuous inhibition of excess stomatal development.
418 Therefore, our profiling most likely captured a pool of ERECTA-family receptors, including both
419 ligand-activated and inactivated states. Furthermore, ligand-induced interactors such as BAK1
420 were also identified, supporting the validity of our approach.
421
422

ACKNOWLEDGEMENTS

We thank Rachael Cox for developing the R package used in this study for differential protein interaction analysis. We also show our gratitude to Kaysa Kerr and Nicole Uwakwe for assisting the screening of transgenic- and T-DNA insertion mutants, Katsunari Maruyama for assisting *in vitro* interaction assays, and Krishna Sepuru and Liangliang Chen for insightful discussion. This work was supported by fundings from the NIGMS (R35GM122480), Army Research Office (W911NF-12-1-0390), and the Welch Foundation (F-1515) to EMM; Japan Society for the Promotion of Science (JSPS) KAKENHI (JP24K02050) and the Takeda Science Foundation to T.U.; Japan Science and Technology Agency (JST) CREST (JPMJCR20E5) and ERATO (JPMJER2403) to K.E; and the Howard Hughes Medical Institute and the start-up fund from The University of Texas at Austin, as well as the Johnson & Johnson Centennial Chair awarded to K.U.T.

AUTHOR CONTRIBUTIONS

Conceptualization, P.B., K.U.T.; Experimental Design, P.B., T.U., E.M.M., K.U.T.; Performance of experiments, P.B., C.K., K.E., A.N.; Bioinformatics Analysis, P.B., O.P., E.M.M.; Visualization, P.B., E.M.M., K.U.T.; Essential materials and tools, P.B., A.N., T.S., T.U.; Writing- Original Draft, P.B. and K.U.T.; Writing- Review & Editing, P.B., C.K., T.U., K.E., O.P., E.M.M., K.U.T; Project Administration, K.U.T.; Funding Acquisition, T.U., K.E., E.M.M., K.U.T.

DECLARATION OF INTERESTS

The authors declare no competing interests.

RESOURCE AVAILABILITY

Lead contact

Further information and requests for resources and reagents should be directed and will be fulfilled by the Lead Contact, Keiko U. Torii (ktorii@utexas.edu).

Materials availability

Plasmids and transgenic plants generated in this study will be available from the lead contact upon request.

Data and code availability

- The mass spectrometry data generated for the proteomic analysis in this study have been deposited to the ProteomeXchange consortium via the partner repository MassIVE (https://massive.ucsd.edu/ProteoSAFe/static/massive.jsp) with the dataset identifier: MSV000096929. Original western blot images are being deposited at Texas Dataverse.
- This paper does not report original code.
- Any additional information required to reanalyze the data reported in this paper is available from the lead contact upon request

EXPERIMENTAL MODEL AND SUBJECT DETAILS

The *Arabidopsis thaliana* Columbia (Col-0) ecotype was used as wild-type control. Loss-of-function T-DNA insertion mutants were obtained from the Arabidopsis Biological Resource Center (ABRC) at The Ohio State University. Higher-order mutants were generated through genetic crosses of single and double mutants, with genotypes confirmed by PCR. Transgenic *Arabidopsis* lines expressing HA-TbID-tagged or fluorescently tagged proteins were generated via the floral dipping method using *Agrobacterium tumefaciens* GV3101::pMP90. Information of recombinant DNA constructs used for plant transformation is provided in Table S1. Primer sequences used for genotyping, cloning, and plasmid construction are listed in Table S2. A complete list of mutants and transgenic lines is included in the Key Resources Table. Seedlings and adult plants were grown in a controlled long-day growth chamber (16 hours light/8 hours dark) at 22 °C during the light phase and 20 °C during the dark phase.

METHOD DETAILS

Plant materials and growth condition

Arabidopsis Col-0 was used as the wild-type control in this study. The following materials have been published previously: *er-105*, *erl1-2, erl2-1, er-105;erl1-2, er-105;erl2-1, erl1-2;erl2-1*, *er-105;erl1-2;erl2-1* [11]; *ARA6pro::ARA6-mRFP, ARA7pro::mRFP-ARA7, SYP22pro::SYP22-mRFP, SYP43pro::SYP43-mRFP* [80]. The following Arabidopsis mutants were obtained from Arabidopsis Biological Resource Center (ABRC): *picalm1a* (SALK_043625); *picalm1b* (GABI_026G05); *picalm2b* (SALK_032696), *picalm3* (WiscDsLoxHs184_04D); *picalm4a* (WiscDsLox442D1); *picalm4b* (SAIL_418_A409); Higher-order mutants of *PICALM* family are generated through genetic crosses, including double mutant *picalm1a;1b*, *picalm4a;4b*, triple mutant *picalm3;4a;4b*,

quadruple mutant *picalm1a;1b;4a;4b*, and quintuple *picalm1a;1b;3;4a;4b*, *picalm1a;1b;2b;3;4b*. Arabidopsis seeds were surface sterilized with 2.5 % sodium hypochlorite solution, stratified at 4 °C in darkness for two days, and then germinated on half-strength Murashige-Skoog (1/2 MS) medium plates for 8-10 days before imaging or transplanting to soil pots. The 1/2MS medium (pH 5.7) contains 1.0 % sucrose, 1x Gamborg′s Vitamins (Sigma, Cat # G1019), and 0.75 % agar. Plants were grown in a controlled growth room under a long-day cycle of 16 hours light (22 °C) and 8 hours dark (20 °C).

Plasmid constructions and plant transformation

The *ERECTA-TurboID* construct pPFB11 (*ERECTApro::ERECTA-HA-TbID*) and the negative control pPFB36 (*ERECTApro::Lti6B-HA-TbID*) were generated using a MultiSite Gateway cloning strategy. Entry vectors containing the *ERECTA* promoter and entry vectors containing either *ERECTA*- or *Lti6B-HA-TbID* fusions were recombined into the R4pGWB501 destination vector [81]. For protoplast expression, genomic coding sequences of *PICALM3*, *PICALM4A*, and *PICALM4B* were PCR-amplified from Col-0 genomic DNA and cloned into the pYBA-1132 vector (35S::C-terminal EGFP, NCBI Accession: KF876796) via *BamHI* and *KpnI* restriction sites. Additionally, the genomic coding sequence of *ERECTA* was cloned into the pHBT-2xHA vector using *BamHI* and *StuI* restriction sites. To generate constructs for the AlphaScreen assay, coding sequences (CDSs) of *PICALM* family genes (*PICALM1A*, *PICALM2B*, *PICALM3*, *PICALM4A*, *PICALM4B*, *PICALM5A*, *PICALM6*, *PICALM8*, *PICALM9B*, *PICALM10B*) and the cytoplasmic kinase domain of *ERECTA* (ER-KD) were PCR-amplified from Col-0 cDNA. The amplified CDSs were cloned into pENTR/D-TOPO entry vectors and recombined into the destination vectors pEU-E01-GW-bls-STOP[82] and pEU-E01-AGIA-GW-STOP[83]. GFP expressed from pEU-E01-AGIA-GW-STOP served as a negative control. Two additional constructs used for subcellular localization and complementation experiments, *PICALM3pro::PICALM3-TagRFP-pGWB559* and *PICALM4apro::PICALM4a-mRFP-pGWB1*, were generated by Gateway cloning. A full list of plasmids and primers used is provided in Tables S1 and S2. Stable transgenic plants were generated using Agrobacterium tumefaciens (GV3101::pMP90) -mediated floral dipping method[84]. At least 20 independent T1 transformants were analyzed for each construct. Stable transgenic lines were identified by segregation analysis for single-locus insertion (3:1 segregation ratio).

Confocal microscopy imaging

Confocal imaging for stomatal phenotyping was conducted using a Leica SP5-WLL microscope equipped with a 20x dry objective lens. Cotyledons from 8 dpg *Arabidopsis* seedlings were stained with 1.0 mg/mL propidium iodide (PI) (Sigma, Cat # P4864) for 1 min to visualize cell outlines. The abaxial epidermis was imaged using an excitation wavelength of 561 nm and an emission detection range of 590-659 nm. Z-stack images spanning the full depth of the epidermal cell layers were captured and processed using Fiji/ImageJ software (http://fiji.sc/Fiji). Maximum intensity projections were generated, and representative images were false-colored and adjusted for brightness and contrast using Adobe Photoshop 2022. For subcellular co-localization and internalization analyses, fluorescent signals were captured using the Leica SP5-WLL with a 63x water immersion objective, or the Leica Stellaris 8 FALCON microscope with 40 x or 63 x oil immersion objectives operated in TauGating mode. Fluorescence excitation/emission settings were optimized for specific fluorophores as follows: YFP (514 nm excitation, 520-550 nm

534 emission), mRFP (584 nm excitation, 600–650 nm emission), and TagRFP (555 nm excitation,
535 565–650 nm emission). For exogenous chemical treatments, four-day old Arabidopsis seedlings
536 were pre-stained in ultrapure water containing 5 μM FM4-64 (Thermo Scientific, Cat. # T3166) for
537 10min. Following staining, seedlings were immersed in ½ MS liquid medium supplemented with
538 30 μM BFA (30 mM stock in ethanol), 30 μM Wortmannin (30 mM stock in DMSO), or 50 μM
539 cycloheximide (100 mg/mL stock in DMSO). Seedlings were vacuum infiltrated for 1 min to
540 facilitate chemical uptake and subsequently incubated for 60 mins prior to imaging. For EPF2
541 ligand-induced internalization analyses, recombinant mEPF2 peptide was purified and refolded
542 to retain its bioactivity. After confirming its bioactivity, the peptide was added into 1/2MS liquid
543 medium, with or without 30 μM Wortmannin. Seedlings were incubated for 90min followed by 8
544 μM FM4-64 staining before imaging.
545
546 **Sample preparation for proximity labeling**
547 TurboID-based proximity labeling assays were conducted following previously described
548 procedures with modification[37,38,40]. Seeds of *ERECTApro::ERECTA-HA-TbID* transgenic lines
549 were surface-sterilized with 70% ethanol and sown on filter paper (90 mm, Cytiva Whatman™,
550 Cat # 09-853A) placed on 1/2 MS medium plates. Five-day-old seedlings grown under long-day
551 conditions were harvested and transferred to a flask for biotin treatment. To optimize labeling
552 conditions, a range of biotin solutions (0, 5, 20, 50, 100, and 250 μM) and incubation durations (0,
553 15 mins, 30 mins, 1 hr, 2 hrs, 3 hrs) were tested. Optimal conditions for the ERECTA-TurboID PL
554 assay were determined to be an incubation with 50 μM biotin for 1 hr at room temperature. To
555 terminate the PL reaction, seedlings were rinsed five times with ice-cold water to remove excess
556 biotin, gently blotted dry with laboratory Kimwipes, and immediately frozen in liquid nitrogen.
557 Frozen samples were ground into a fine powder under liquid nitrogen for protein extraction. All
558 experiments were performed in three independent biological replicates.
559 Approximately 2.0 mL of the finely ground samples were homogenized in 2.5 mL of ice-
560 cold protein lysis buffer (100 mM Tris pH 7.5, 150 mM NaCl, 10 % glycerol, 20 mM Sodium fluoride,
561 1.5 mM Sodium orthovanadate, 2 mM Sodium molybdate, 1 mM PMSF, 1 % Triton x-100, 1x
562 Protease inhibitor cocktail) in a 5.0 mL LoBind tube (Eppendorf, 0030108302). The mixture was
563 incubated on a rotor wheel at 4 °C for 30 min and then sonicated four times at 4 °C for 30s with
564 90s intervals on a high setting using a Bioruptor 300 (Diagenode). Next, the homogenized
565 samples were centrifuged at 13,000 rpm for 10 mins at 4 °C to remove cell debris. Approximately
566 2.5 mL of the supernatant was processed through a PD-10 desalting column (Cytiva, Cat # 17-
567 0851-01) using the gravity flow protocol to remove excess free biotin. Approximately 3.5 mL of
568 protein extract was collected, and the protein concentration was determined using the Bradford
569 assay (Bio-Rad). The protein extracts were divided equally for the analysis of the ERECTA
570 proximitome and interactome. For proximitome, 1.7 mL of lysate (approximately 5.5 mg of protein)
571 was transferred to a new 2.0 mL LoBind tube (Eppendorf, 0030108450) and incubated with 100
572 μL of pre-equilibrated streptavidin magnetic beads (Thermo Scientific, Cat # 88817) at 4°C for 18
573 hrs on a rotor wheel. The streptavidin magnetic beads, enriched with biotinylated proteins, were
574 sequentially washed three times with protein lysis buffer, followed by washes with 1 M KCl, 0.1 M
575 Na_2CO_3, 2 M urea, and 50 mM Tris-HCl (pH 8.0). One-tenth of the beads were used for Western
576 blot analysis, and the remaining beads were frozen for subsequent analysis. Similarly, the second
577 portion (5.5 mg of protein), was incubated with 100 μL of pre-equilibrated anti-HA magnetic beads

578 (Thermo Scientific, Pierce™, Cat # 88837) under the same conditions. The anti-HA magnetic
579 beads were washed three times with protein lysis buffer and three times with 50 mM Tris-HCl (pH
580 8.0). One-tenth of the beads were used for Western blot analysis, and the remaining beads were
581 frozen for subsequent analysis.
582
583 **LC-MS sample preparation**
584 Biotinylated proteins bound to streptavidin magnetic beads were processed for mass
585 spectrometry analysis using an on-bead trypsin digestion protocol. The streptavidin magnetic
586 bead samples, previously stored at -80 °C, were thawed and washed three times with 50 mM
587 Tris-HCl buffer (pH 8.0) to remove excess detergents and salts. An equal volume of
588 trifluoroethanol (TFE) was added to denature the proteins and expose trypsin cleavage sites.
589 Tris(2-carboxyethyl) phosphine (TCEP) was added to a final concentration of 5 µM, and the
590 mixture was incubated at 55°C for 45 mins to reduce disulfide bonds. After cooling to room
591 temperature, iodoacetamide (15 mM final concentration) was added to alkylate cysteine residues
592 and prevent the reformation of disulfide bonds. This reaction was conducted in the dark at room
593 temperature for 30 mins and quenched with 7 mM dithiothreitol (DTT). For trypsin digestion, the
594 mixture was diluted with 50 mM Tris-HCl (pH 8.0) containing 2 mM $CaCl_2$ and 2.0 µg MS-grade
595 trypsin (Thermo Scientific, Cat # 90058). The digestion reaction was incubated at 37 °C for 5 hrs
596 with end-to-end rotation and terminated by adding formic acid to a final concentration of 1% (v/v).
597 Protein complexes enriched with anti-HA magnetic beads were eluted by washing the beads three
598 times with 0.1 M glycine (pH 2.5), followed by separation of the supernatant from the bead pellet.
599 The eluate was neutralized with 1M Tris-HCl buffer (pH 8.0) and subjected to the same trypsin
600 digestion protocol as described above. After trypsin digestion, the supernatant was separated
601 from the bead pellet and concentrated using a vacuum concentrator (Vacufuge plus, Eppendorf).
602 The sample was desalted using C18 pipette tips (Thermo, Cat # 60109-412), dried in a SpeedVac,
603 and resuspended in buffer (5 % acetonitrile, 95 % LC-MS grade water with 0.1 % formic acid) for
604 liquid chromatography-mass spectrometry (LC-MS) analysis.
605
606 **Mass spectrometry data analysis**
607 Raw MS/MS spectra were acquired using a Thermo Orbitrap Fusion Lumos mass spectrometer
608 and processed using Proteome Discoverer (version 2.3) following the PWF_Basic_SequestHT
609 workflow with the Percolator node for peptide spectrum match (PSM) validation. The processing
610 settings included trypsin digestion with up to two missed cleavages, static modifications of
611 carbamidomethyl cysteine, dynamic modifications of oxidized methionine, and protein N-terminal
612 modifications of acetylation and/or methionine-loss. Mass spectra were searched against the
613 Arabidopsis thaliana (ARATH) reference proteome, TurboID, and common contaminants
614 (downloaded from https://www.uniprot.org). High-confidence PSMs, peptides, and proteins were
615 all filtered at a false discovery rate of < 5%. Individual RAW files were processed to generate .msf
616 files, which were reprocessed together using the CWF_Basic workflow with Merge Mode set to
617 "Do Not Merge" to generate a single consensus file for comparative analysis. Proteins significantly
618 associated with ERECTA bait were identified by calculating $\log_2$ fold-changes and Z-scores based
619 on observed PSMs between experimental and control conditions, using the R package diffprot
620 (https://github.com/rachaelcox/diffprot.git).
621

622 **Protein Interaction network construction**
623 Proteins significantly enriched in the TurboID-PL and ET-AP datasets (Table S3, S4 and S5) were
624 selected and mapped to the STRING database (https://string-db.org/) using a medium confidence
625 score threshold (interaction score ⩾ 0.4). The resulting protein-protein interaction (PPI) network
626 was visualized in Cytoscape (version 3.9.1)[85], with edges representing both experimentally
627 determined and computationally predicted interactions (e.g., gene neighborhood, fusions, and co-
628 occurrence). Node colors were used to distinguish the proteomic approaches, while node size
629 reflected interaction degree. Functional clusters were manually curated to highlight key biological
630 processes, including internalization, exocytosis, and stomatal development, based on Gene
631 Ontology (GO) annotations and pathway analysis.
632
633 **Protoplast transfection assay**
634 The isolation and transfection of Arabidopsis protoplasts were performed with minor modifications
635 to the protocol as previously described[86]. Arabidopsis Col-0 plants were grown under short-day
636 conditions (8 hrs light at 22 °C/ 16 hrs dark at 20 °C). For protoplast isolation, rosette leaves from
637 4-week-old plants were cut into 0.5-1.0 mm strips and digested in an enzymatic solution
638 containing 1 % Cellulase R10 (Yakult Honsha, Japan), 0.2 % Macerozyme R10 (Yakult Honsha,
639 Japan), 0.4 M mannitol, 20 mM KCl, 20 mM MES, 10 mM $CaCl_2$, 5 mM β-mercaptoethanol, and
640 0.1 % BSA. Digestion was carried out with gentle shaking (40 rpm) for 3 hrs in the dark. The
641 protoplasts were collected by filtering the solution through a 70 µm nylon mesh (Corning, Cat #
642 352350) and washed three times with W5 solution (154 mM NaCl, 125 mM CaCl2, 5 mM KCl, 5
643 mM glucose, 2 mM MES, pH 5.7) to remove residual enzymes. The protoplasts were resuspended
644 in MMG solution (400 mM mannitol, 15 mM MgCl2, 4 mM MES, pH 5.7) for transfection. For PEG-
645 mediated transfection, 200 µL of protoplast suspension (5×10^5 cells/mL) was mixed with 10-15
646 µg of plasmid DNA in a 1.5 mL Eppendorf LoBind tube. The mixture was incubated with an equal
647 volume of freshly prepared PEG solution (40% PEG 4000 w/v, 0.2 M mannitol, 0.1 M CaCl2) for
648 10 minutes at room temperature. Transfection was stopped by adding double volume of W5
649 solution, followed by gentle centrifugation to pellet the protoplasts. The protoplasts were
650 resuspended in W5 solution and incubated in the dark for 12 hours at plant growth room.
651
652 **Co-Immunoprecipitation (Co-IP) assays**
653 The Co-IP assay was conducted with minor modifications to the protocol[87]. Protoplast samples
654 were suspended in 1.0 mL of ice-cold Co-IP buffer (100 mM Tris-HCl, pH 7.5, 150 mM NaCl, 1
655 mM EDTA, 1 % Triton X-100, 3 mM DTT, 1 mM PMSF, 1 x protease inhibitor cocktail) in a 1.5 mL
656 LoBind tube. The samples were centrifuged at 13000 rpm for 10 mins at 4 °C to remove cell debris.
657 A 45 µL aliquot of the supernatant was mixed with 15 µL of 4× Laemmli buffer and saved as the
658 input sample. The remaining supernatant was transferred to a new 1.5 mL LoBind tube containing
659 20 µL of GFP-Trap magnetic agarose (ChromoTek, Cat # gtma-100) and incubated on an end-
660 to-end rotor at 4 °C for 1 hr. After incubation, the GFP-Trap agarose beads were separated using
661 a magnetic rack and washed three times with Co-IP buffer, followed by a final wash with 50 mM
662 Tris-HCl (pH 8.0). The beads were resuspended in 30 µL of 50 mM Tris-HCl and mixed with 10
663 µL of 4 x Laemmli buffer. The mixture was boiled for 5 min and analyzed by immunoblotting.
664
665 **AlphaScreen-based protein-protein interaction assay**

666 The AlphaScreen assay is a robust proximity-based approach to detect biomolecular interactions
667 *in vitro*[62]. It relies on the energy transfer between donor and acceptor beads brought into proximity
668 by the binding of tagged proteins, resulting in a luminescent signal proportional to the interaction
669 strength. The promoter, CDS, and terminator regions of the *PICALM-bls*, *AGIA-ERendo*, and
670 *GFP-AGIA* constructs were amplified via PCR with SPu and AODA2306 primers and used as
671 templates for *in vitro* transcription and translation in a wheat germ cell-free system (No Cat # CFS-
672 TRI-1240, CellFree Sciences, Japan). Biotinylation at the biotin ligation site (bls) was performed
673 enzymatically with BirA biotin ligase and 0.5 μM d-biotin (No Cat # 04822-04, Nacalai Tesque,
674 Japan) as previously described[88]. Protein synthesis was confirmed by immunoblotting with HRP-
675 conjugated anti-AGIA (1:10,000) and anti-biotin (1:1,000, Cell Signaling Technology) antibodies.
676 AlphaScreen reactions were performed with slight modifications to the protocol[89]. A 15 μL reaction
677 containing AlphaScreen buffer (100 mM Tris-HCl, pH 8.0, 0.1% Tween-20, 1 mg/mL BSA), 1 μL
678 monobiotinylated PICALMs, and 1 μL AGIA-tagged ER-KD or GFP was incubated at 26°C for 1
679 hour in an Optiplate-384 plate (Revvity). A 10 μL detection mixture containing streptavidin-
680 conjugated donor beads, protein A-conjugated acceptor beads, and anti-AGIA antibody in
681 AlphaScreen buffer was then added. After an additional 1-hour incubation at 26°C,
682 chemiluminescence signals were measured using an EnVision 2105 multimode plate reader
683 (Revvity).
684
685 **Immunoblot analysis**
686 Protein samples were resolved on 8 - 10% SDS-PAGE gels and transferred to PVDF membranes
687 (BioRad Cat # 1620177). Membranes blocked in 5% nonfat milk in TBST for 1 hr at room
688 temperature, followed by overnight incubation at 4 °C with primary antibodies, including anti-HA
689 (1:5000, Abcam, Cat # Ab18181), anti-GFP (1:5000, Invitrogen, Cat # 33-2600), anti-RFP (1:2000,
690 ChromoTek, Cat # pabr1), and anti-ACTIN (1:10,000, Abcam, Cat # Ab230169). After washing,
691 membranes were incubated with HRP-conjugated secondary antibodies (1:10,000, Jackson
692 ImmunoResearch Labs, Cat # 112-035-003 for rat, Cat # 115-035-062 for mouse) for 1 hr at room
693 temperature. For PL samples, membranes were incubated with horseradish peroxidase conjugate
694 streptavidin (1:5000, Invitrogen, Cat # S911). Protein bands were detected using
695 chemiluminescence ECL substrate and imaged with a Bio-Rad ChemiDoc system.
696
697 **qRT-PCR analysis**
698 Total RNA extraction, first-strand cDNA synthesis and qRT-PCR were performed as previously
699 described[74]. Gene expression levels were quantified using relative $2^{-\Delta CT}$ method with the
700 Arabidopsis *ACT2* (AT3G18780) as the endogenous reference for normalization. Primer
701 sequences used were listed in Table S2.
702
703 **QUANTIFICATION AND STATISTICAL ANALYSIS**
704 To quantitatively analyze the stomatal phenotypes of mutants and complementation lines, the
705 abaxial side of Arabidopsis cotyledons was imaged using confocal microscopy. The images were
706 used to classify and count different epidermal cell types. The stomatal index, defined as the
707 number of stomata divided by the total number of epidermal cells, was calculated. The stomatal
708 cluster index, representing the proportion of stomatal groups with two or more adjacent stomata,
709 were calculated as the ratio of stomata in cluster groups to the total number of stomata. For each

genotype, 18 - 20 cotyledons encompassing over 1500 epidermal cells were analyzed to ensure statistical robustness. To quantitatively analyze the AlphaScreen results, the mean chemiluminescence signals from three replicates were calculated and compared between ERECTA and GFP reactions. For mass spectrometry data, protein fold-changes were calculated as log2-transformed ratios of normalized PSMs between experimental and control conditions. Protein enrichment significance was assessed using a one-sided Z-test[90] with a 95% confidence threshold ($z \geqslant 1.645$). *p*-values were calculated using the pnorm function in R (version 4.2.2) and adjusted for multiple comparisons using the Benjamini-Hochberg false discovery rate correction as previous described[91]. Statistical analyses and data visualization were performed using R. For the two-sample comparison, either student's t-test or Welch's t-test were performed. For the multiple sample comparison, one-way ANOVA with post-hoc Tukey HSD test was performed. The corresponding *p*-values and sample size (n) are provided in the respective figure legends.

FIGURE LEGENDS

Figure 1. Comparative proteomic profiling of ERECTA-associated proteins.

(A) Schematic representation of the experimental workflow for profiling ERECTA-associated proteins using TbID-PL and ET-AP. Parallel enrichments of biotinylated proteins and HA-tagged protein complexes were subjected to mass spectrometry analysis.

(B) Immunoblot validation of ERECTA and its associated proteins. Streptavidin-HRP (SA-HRP) (top) confirms successful biotinylation of proximal proteins via TbID-PL. α-HA immunoblot (middle) verifies the expression and enrichment of ERECTA-HA-TbID. Ponceau S staining (bottom) indicates loading control.

(C) Venn diagram of identified proteins reveals 665 unique to TbID-PL, 228 unique to ET-AP, and 50 shared proteins.

(D) Subcellular localization of TbID-PL enriched proteins, showing enrichment at the plasma membrane and cytosol, with additional representation in endomembrane compartments.

(E) Scatterplot comparing protein enrichment between TbID-PL and ET-AP. Notable components of clathrin-mediated endocytosis (CME), such as PICALMs, DRPs, and TPLATE complex members, are preferentially captured by TbID-PL. In contrast, stable receptor partners like TMM are enriched via ET-AP. Some auxin transporters (PIN3, PIN7) are recovered in both methods.

(F) GO-term enrichment of TbID-PL-identified proteins reveals overrepresentation of membrane trafficking, endocytosis, protein localization, and epidermal development terms. Circle size represents fold enrichment; color indicates false discovery rate (FDR) values.

746 **Figure 2. Optimized TbID-PL enhances detection of ERECTA-associated signaling**
747 **components and compartment-specific proteomes.**
748 (A) Scatterplot showing differential enrichment of biotinylated proteins in ERECTA-TbID-PL with
749 biotin versus without biotin treatments. Several known ERECTA signaling components, including
750 BAK1, YODA (MAPKKK4) are identified (orange) alongside clathrin-mediated endocytosis
751 proteins (e.g., PICALM4A, PICALM4B) identified (green) in Figure 1.
752 (B) Scatterplot comparing enrichment between microsomal and cytosolic fractionation in TbID-PL
753 proteomes. Membrane-attached receptor-like cytoplasmic kinase BSK1 is predominantly
754 enriched in the microsomal fraction, while CME components (e.g., PICALM4A, 4B) and ERECTA
755 are detected in both fractions.
756 (C) Venn diagram showing overlap among TbID-PL datasets derived from comparisons of
757 ERECTA-HA-TbID vs *er-105*, +biotin vs -biotin, and microsomal vs cytosolic fractions. Seven
758 candidates are consistently detected across all comparisons.
759 (D) Heatmap showing normalized enrichment (log2 z-scores) of the top 7 consistently identified
760 ERECTA-proximal proteins across four TbID-PL conditions. These include ERECTA itself,
761 PICALM4A/B, and kinases implicated in receptor signaling (LIK1, HERK1, TMK4), as well as
762 ANGUSTIFOLIA and PHOT1.
763 (E) STRING network analysis of ERECTA-associated proteins identified by TbID-PL (green),
764 optimized TbID-PL (orange), or ET-AP (blue). Proteins are clustered into major functional
765 categories: internalization/protein trafficking, exocytosis, motor proteins, and stomatal
766 development. ERECTA, CME components (PICALMs, TPLATE, DRPs), and signaling partners
767 (e.g., BAK1, YODA, TMM) are highlighted. Node size reflects interaction confidence.
768
769 **Figure 3. ERECTA selectively interacts with PICALM family of clathrin-mediated**
770 **endocytosis (CME) components.**
771 (A) Dot plot showing transcriptional expression of Arabidopsis PICALM family genes across
772 stomatal lineage cell types from re-analyzed single-cell RNA-seq data. PICALM1, PICALM3,
773 PICALM4A, and PICALM4B are present across different stages of stomatal lineage cells.
774 PICALM1, PICALM4A, and PICALM4B are highly enriched in guard mother cell (GMC), guard
775 cell (GC) stages, while PICALM2B and PICALM3 are highly enriched in stomatal lineage ground
776 cells (SLGCs). The distinct expression of PICALMs suggest their potential roles in different stage
777 of stomatal development. Dot size indicates proportion of expressing cells; dot color reflects
778 expression levels.

779 (B) Phylogenetic tree of Arabidopsis PICALM family members. PICALM3 (Group 1, blue) and
780 PICALM4A/B (Group 2a, green) cluster into distinct clades with high proximity to ERECTA based
781 on TbID-PL. The phylogenetic tree illustrates evolutionary relationships and potential functional
782 specialization within PICALM family.
783 (C) Confocal microscopy showing subcellular colocalization of endogenous promoters-driven
784 ERECTA-YFP and PICALM4A-RFP in cotyledon epidermal cells at multiple stomatal lineage
785 stages. M, meristemoid; GMC, guard mother cell; GC, guard cell. Scale bars, 10 μm. ERECTA-
786 YFP colocalizes with PICALM4A-RFP at the plasma membrane in stomatal lineage cells, except
787 at cell plates for dividing cells.
788 (D) *In vitro* protein-protein interacting assay between ERECTA and PICALM family proteins.
789 ERECTA cytoplasmic domain and PICALMs were *in vitro* translated for the AlphaScreen assay.
790 Quantification of normalized binding activity (right) confirms the preferential binding for PICALM3,
791 PICALM4A, and PICALM1A. Boxplots represent mean with SD from three biological replicates
792 and significance was assessed by unpaired t-test.
793 (E) Co-immunoprecipitation assays validating interactions between ERECTA and PICALM
794 proteins transiently co-expressed in Arabidopsis protoplasts. Immunoblot analysis confirmed *in-*
795 *vivo* binding of ERECTA-HA to PICALM3-GFP, PICALM4A-GFP, and PICALM4B-GFP, as shown
796 in the red-boxed lanes.
797
798 **Figure 4. ERECTA-YFP co-localizes with PICALM4A and endosomal markers in stomatal-**
799 **lineage cells.**
800 (A) Confocal microscopy showing colocalization of ERECTA-YFP with PICALM4A-RFP under
801 mock and BFA-treated conditions. In untreated cells, both proteins localize to the plasma
802 membrane. Brefeldin A (BFA) treatment results in BFA-induced endosomal compartments, where
803 PICALM4A-RFP encapsulates and colocalizes with ERECTA-YFP (arrowheads).
804 (B) Confocal microscopy showing that ERECTA-YFP does not colocalize with the plasma
805 membrane marker RCI2A-mCherry in BFA bodies. Under BFA treatment, ERECTA-YFP is
806 redistributed to endosomal compartments (arrowheads), while RCI2A-mCherry remains at the
807 plasma membrane, indicating selective internalization of ERECTA.
808 (C) Confocal microscopy imaging of ERECTA-YFP with the trans-Golgi network (TGN) marker
809 SYP43-RFP (top) and the plasma membrane/early endosome marker ARA6-RFP (bottom). Under
810 mock conditions, ERECTA-YFP localizes to the plasma membrane and partially colocalizes with
811 SYP43 and ARA6 (arrowheads). Following BFA treatment, ERECTA-YFP colocalized with both

812 SYP43-RFP and ARA6-RFP in BFA-induced endosomal compartments, confirming its trafficking
813 through the TGN and early endosomes.
814 (D) Confocal microscopy showing colocalization of ERECTA-YFP with the late endosome marker
815 ARA7-RFP and the vacuolar membrane marker SYP22-RFP. Under mock conditions, limited
816 colocalization is observed. Upon wortmannin treatment, ERECTA-YFP co-localizes with ARA7-
817 RFP in these enlarged endosomes, indicating ERECTA's progression toward late endosome and
818 vacuoles.
819
820 **Figure 5. PICALM proteins regulate ERECTA internalization.**
821 (A) Confocal images of ERECTA-YFP internalization in WT and *picalm1a;1b;4a;4b* mutants under
822 mock and BFA treatment. In WT, BFA induces the formation of ERECTA-YFP–positive
823 endosomal compartments (BFA bodies, arrowheads). Whereas the number of BFA body is
824 markedly reduced in the *picalm1a;1b;4a;4b* mutant, indicating impaired endocytic recycling.
825 (B) Quantification of the number of cells with BFA bodies across stomatal lineage stages in WT.
826 ERECTA-YFP endocytic activity is enriched in pavement cells (PCs) and stomatal lineage ground
827 cells (SLGCs).
828 (C) Box plot quantifying the number of BFA bodies per cell under mock and BFA treatments in
829 WT and *picalm1a;1b;4a;4b* mutants. WT shows a significant increase in BFA bodies upon
830 treatment, while *picalm1a;1b;4a;4b* mutant exhibits no significant response.
831 (D) Confocal microscopy images showing ERECTA-YFP internalization in response to mEPF2
832 peptide, wortmannin, or their combination in WT and *picalm1a;1b;4a;4b* mutants. In WT, mEPF2
833 triggers endocytic accumulation of ERECTA-YFP that overlaps with FM4-64, and Wm enlarges
834 late endosomes containing ERECTA-YFP. These responses are strongly reduced in the
835 *picalm1a;1b;4a;4b* mutant (arrowheads).
836 (E) Quantification of mEPF2-induced ERECTA-YFP puncta in WT and *picalm1a;1b;4a;4b*
837 mutants shows impaired ligand-triggered ERECTA endocytosis in the mutant.
838 (F) Quantification of ERECTA-YFP positive Wm bodies per cell in WT and *picalm1a;1b;4a;4b*
839 mutant. Wm-induced accumulation is significantly reduced in the mutant, indicating defective
840 trafficking to late endosomes.
841
842 **Figure 6. *PICALMs* are required for proper stomatal patterning**
843 (A) Confocal images of abaxial epidermis from wild-type (WT) and various *picalm* single, double,
844 and higher-order mutants. WT plants exhibit normal stomatal development, whereas *picalm*

845 mutants exhibit increased stomatal index with varying degrees of stomatal clustering. Scale bars,
846 40 µm.
847 (B) Quantification of stomatal index in WT and *picalm* mutants. Box plots show a significant
848 increase in stomatal index in *picalm* mutants compared to WT. Statistical analysis was determined
849 using one-way ANOVA followed by Tukey's HSD test.
850 (C) Stomatal cluster index analysis in WT and *picalm* mutants. Stomatal clusters are categorized
851 by size (e.g., two, three, or four stomata per cluster), highlighting a dramatic rise in clustering
852 frequency in higher-order *picalm* mutants.
853 (D) Confocal images of abaxial epidermis from WT, *er-105*, *picalm1a;1b;4a;4b*, and the quintuple
854 mutant *picalm1a;1b;4a;4b;er-105*. The quintuple mutant shows similar stomatal numbering and
855 clustering to *er-105*. Scale bars, 40 µm.
856 (E) Quantification of combined stomatal and meristemoid index. The *picalm1a;1b;4a;4b;er-105*
857 quintuple mutant exhibits values comparable to *er-105*, indicating that PICALMs act in the same
858 genetic pathway as ERECTA.
859 (F) Proposed model of the ERECTA receptor internalization facilitated by PICALM proteins.
860 ERECTA is internalized through CME involving adaptor proteins such as PICALM3, PICALM4A,
861 and PICALM4B, along with the AP2 complex and TPLATE. Internalized receptors are sorted via
862 early endosomes or the trans-Golgi network (TGN) for recycling, or trafficked to vacuoles for
863 degradation. In *picalm* mutants, defective CME impairs receptor pool balance, disrupting stomatal
864 patterning. The secretion of newly synthesized ERECTA and trafficking to late
865 endosomes/vacuoles remain unresolved in *picalm* mutants.
866 (G) Representative images comparing stomatal patterning in WT, *picalms, er,* and *er; erl1; erl2*
867 mutants. *picalm* mutants phenocopy *er* family mutants, displaying increased stomatal number and
868 clustering, supporting a functional link between CME regulation and ERECTA-mediated signaling.
869

870 **REFERENCES**
871

872 1. Torii, K.U. (2004). Leucine-rich repeat receptor kinases in plants: structure, function, and
873 signal transduction pathways. Int Rev Cytol *234*, 1-46. 10.1016/S0074-7696(04)34001-5.
874 2. Shiu, S.H., and Bleecker, A.B. (2001). Receptor-like kinases from Arabidopsis form a
875 monophyletic gene family related to animal receptor kinases. Proc Natl Acad Sci U S A
876 *98*, 10763-10768. 10.1073/pnas.181141598.
877 3. Boutrot, F., and Zipfel, C. (2017). Function, Discovery, and Exploitation of Plant Pattern
878 Recognition Receptors for Broad-Spectrum Disease Resistance. Annu Rev Phytopathol
879 *55*, 257-286. 10.1146/annurev-phyto-080614-120106.
880 4. Nolan, T.M., Vukasinovic, N., Liu, D., Russinova, E., and Yin, Y. (2020). Brassinosteroids:
881 multidimensional regulators of plant growth, development, and stress responses. Plant
882 Cell *32*, 295-318. 10.1105/tpc.19.00335.
883 5. Chen, X., Ding, Y., Yang, Y., Song, C., Wang, B., Yang, S., Guo, Y., and Gong, Z. (2021).
884 Protein kinases in plant responses to drought, salt, and cold stress. J Integr Plant Biol *63*,
885 53-78. 10.1111/jipb.13061.
886 6. Escocard de Azevedo Manhaes, A.M., Ortiz-Morea, F.A., He, P., and Shan, L. (2021).
887 Plant plasma membrane-resident receptors: Surveillance for infections and coordination
888 for growth and development. J Integr Plant Biol *63*, 79-101. 10.1111/jipb.13051.
889 7. Li, J., and Chory, J. (1997). A putative leucine-rich repeat receptor kinase involved in
890 brassinosteroid signal transduction. Cell *90*, 929-938. 10.1016/s0092-8674(00)80357-8.
891 8. Gómez-Gómez, L., and Boller, T. (2000). FLS2: an LRR receptor-like kinase involved in
892 the perception of the bacterial elicitor flagellin in Arabidopsis. Mol Cell *5*, 1003-1011.
893 9. van Zanten, M., Snoek, L.B., Proveniers, M.C., and Peeters, A.J. (2009). The many
894 functions of ERECTA. Trends Plant Sci *14*, 214-218. 10.1016/j.tplants.2009.01.010.
895 10. Shpak, E.D. (2013). Diverse roles of ERECTA family genes in plant development. J Integr
896 Plant Biol *55*, 1238-1250. 10.1111/jipb.12108.
897 11. Shpak, E.D., Berthiaume, C.T., Hill, E.J., and Torii, K.U. (2004). Synergistic interaction of
898 three ERECTA-family receptor-like kinases controls Arabidopsis organ growth and flower
899 development by promoting cell proliferation. Development *131*, 1491-1501.
900 10.1242/dev.01028.
901 12. Shpak, E.D., McAbee, J.M., Pillitteri, L.J., and Torii, K.U. (2005). Stomatal patterning and
902 differentiation by synergistic interactions of receptor kinases. Science *309*, 290-293.
903 10.1126/science.1109710.
904 13. Hara, K., Kajita, R., Torii, K.U., Bergmann, D.C., and Kakimoto, T. (2007). The secretory
905 peptide gene EPF1 enforces the stomatal one-cell-spacing rule. Genes Dev *21*, 1720-
906 1725. 10.1101/gad.1550707.
907 14. Hara, K., Yokoo, T., Kajita, R., Onishi, T., Yahata, S., Peterson, K.M., Torii, K.U., and
908 Kakimoto, T. (2009). Epidermal cell density is autoregulated via a secretory peptide,
909 EPIDERMAL PATTERNING FACTOR 2 in Arabidopsis leaves. Plant Cell Physiol *50*,
910 1019-1031. 10.1093/pcp/pcp068.
911 15. Kondo, T., Kajita, R., Miyazaki, A., Hokoyama, M., Nakamura-Miura, T., Mizuno, S.,
912 Masuda, Y., Irie, K., Tanaka, Y., Takada, S., et al. (2010). Stomatal density is controlled
913 by a mesophyll-derived signaling molecule. Plant Cell Physiol *51*, 1-8.
914 10.1093/pcp/pcp180.
915 16. Lee, J.S., Kuroha, T., Hnilova, M., Khatayevich, D., Kanaoka, M.M., McAbee, J.M.,
916 Sarikaya, M., Tamerler, C., and Torii, K.U. (2012). Direct interaction of ligand-receptor
917 pairs specifying stomatal patterning. Genes Dev *26*, 126-136. 10.1101/gad.179895.111.
918 17. Horst, R.J., Fujita, H., Lee, J.S., Rychel, A.L., Garrick, J.M., Kawaguchi, M., Peterson,
919 K.M., and Torii, K.U. (2015). Molecular framework of a regulatory circuit initiating two-

920 dimensional spatial patterning of stomatal lineage. PLoS Genet *11*, e1005374.
921 10.1371/journal.pgen.1005374.
922 18. Sugano, S.S., Shimada, T., Imai, Y., Okawa, K., Tamai, A., Mori, M., and Hara-Nishimura,
923 I. (2010). Stomagen positively regulates stomatal density in Arabidopsis. Nature *463*, 241-
924 244. 10.1038/nature08682.
925 19. Lee, J.S., Hnilova, M., Maes, M., Lin, Y.C., Putarjunan, A., Han, S.K., Avila, J., and Torii,
926 K.U. (2015). Competitive binding of antagonistic peptides fine-tunes stomatal patterning.
927 Nature *522*, 439-443. 10.1038/nature14561.
928 20. Nadeau, J.A., and Sack, F.D. (2002). Control of stomatal distribution on the Arabidopsis
929 leaf surface. Science *296*, 1697-1700. 10.1126/science.1069596.
930 21. Abrash, E.B., Davies, K.A., and Bergmann, D.C. (2011). Generation of signaling specificity
931 in Arabidopsis by spatially restricted buffering of ligand-receptor interactions. Plant Cell
932 *23*, 2864-2879. 10.1105/tpc.111.086637.
933 22. Lin, G., Zhang, L., Han, Z., Yang, X., Liu, W., Li, E., Chang, J., Qi, Y., Shpak, E.D., and
934 Chai, J. (2017). A receptor-like protein acts as a specificity switch for the regulation of
935 stomatal development. Genes Dev *31*, 927-938. 10.1101/gad.297580.117.
936 23. Meng, X., Chen, X., Mang, H., Liu, C., Yu, X., Gao, X., Torii, K.U., He, P., and Shan, L.
937 (2015). Differential Function of Arabidopsis SERK Family Receptor-like Kinases in
938 Stomatal Patterning. Curr Biol *25*, 2361-2372. 10.1016/j.cub.2015.07.068.
939 24. Chen, L., Maes, M., Cochran, A.M., Avila, J.R., Derbyshire, P., Sklenar, J., Haas, K.M.,
940 Villen, J., Menke, F.L.H., and Torii, K.U. (2025). Preventing inappropriate signals pre- and
941 post-ligand perception by a toggle switch mechanism of ERECTA. Proc Natl Acad Sci U
942 S A *122*, e2420196122. 10.1073/pnas.2420196122.
943 25. Neu, A., Eilbert, E., Asseck, L.Y., Slane, D., Henschen, A., Wang, K., Burgel, P.,
944 Hildebrandt, M., Musielak, T.J., Kolb, M., et al. (2019). Constitutive signaling activity of a
945 receptor-associated protein links fertilization with embryonic patterning in Arabidopsis
946 thaliana. Proc Natl Acad Sci U S A *116*, 5795-5804. 10.1073/pnas.1815866116.
947 26. Claus, L.A.N., Savatin, D.V., and Russinova, E. (2018). The crossroads of receptor-
948 mediated signaling and endocytosis in plants. J Integr Plant Biol *60*, 827-840.
949 10.1111/jipb.12672.
950 27. Geldner, N., Hyman, D.L., Wang, X., Schumacher, K., and Chory, J. (2007). Endosomal
951 signaling of plant steroid receptor kinase BRI1. Genes Dev *21*, 1598-1602.
952 10.1101/gad.1561307.
953 28. Irani, N.G., Di Rubbo, S., Mylle, E., Van den Begin, J., Schneider-Pizon, J., Hnilikova, J.,
954 Sisa, M., Buyst, D., Vilarrasa-Blasi, J., Szatmari, A.M., et al. (2012). Fluorescent
955 castasterone reveals BRI1 signaling from the plasma membrane. Nat Chem Biol *8*, 583-
956 589. 10.1038/nchembio.958.
957 29. Robatzek, S., Chinchilla, D., and Boller, T. (2006). Ligand-induced endocytosis of the
958 pattern recognition receptor FLS2 in Arabidopsis. Genes Dev *20*, 537-542.
959 10.1101/gad.366506.
960 30. Beck, M., Heard, W., Mbengue, M., and Robatzek, S. (2012). The INs and OUTs of pattern
961 recognition receptors at the cell surface. Curr Opin Plant Biol *15*, 367-374.
962 10.1016/j.pbi.2012.05.004.
963 31. Mbengue, M., Bourdais, G., Gervasi, F., Beck, M., Zhou, J., Spallek, T., Bartels, S., Boller,
964 T., Ueda, T., Kuhn, H., and Robatzek, S. (2016). Clathrin-dependent endocytosis is
965 required for immunity mediated by pattern recognition receptor kinases. Proc Natl Acad
966 Sci U S A *113*, 11034-11039. 10.1073/pnas.1606004113.
967 32. Qi, X., Yoshinari, A., Bai, P., Maes, M., Zeng, S.M., and Torii, K.U. (2020). The manifold
968 actions of signaling peptides on subcellular dynamics of a receptor specify stomatal cell
969 fate. Elife *9*. 10.7554/eLife.58097.

33. Smakowska-Luzan, E., Mott, G.A., Parys, K., Stegmann, M., Howton, T.C., Layeghifard, M., Neuhold, J., Lehner, A., Kong, J., Grunwald, K., et al. (2018). An extracellular network of Arabidopsis leucine-rich repeat receptor kinases. Nature *553*, 342-346. 10.1038/nature25184.
34. Tang, W., Kim, T.W., Oses-Prieto, J.A., Sun, Y., Deng, Z., Zhu, S., Wang, R., Burlingame, A.L., and Wang, Z.Y. (2008). BSKs mediate signal transduction from the receptor kinase BRI1 in Arabidopsis. Science *321*, 557-560. 10.1126/science.1156973.
35. Kadota, Y., Sklenar, J., Derbyshire, P., Stransfeld, L., Asai, S., Ntoukakis, V., Jones, J.D., Shirasu, K., Menke, F., Jones, A., and Zipfel, C. (2014). Direct regulation of the NADPH oxidase RBOHD by the PRR-associated kinase BIK1 during plant immunity. Mol Cell *54*, 43-55. 10.1016/j.molcel.2014.02.021.
36. Kerbler, S.M., Natale, R., Fernie, A.R., and Zhang, Y. (2021). From affinity to proximity techniques to investigate protein complexes in plants. Int J Mol Sci *22*. 10.3390/ijms22137101.
37. Branon, T.C., Bosch, J.A., Sanchez, A.D., Udeshi, N.D., Svinkina, T., Carr, S.A., Feldman, J.L., Perrimon, N., and Ting, A.Y. (2018). Efficient proximity labeling in living cells and organisms with TurboID. Nat Biotechnol *36*, 880-887. 10.1038/nbt.4201.
38. Mair, A., Xu, S.L., Branon, T.C., Ting, A.Y., and Bergmann, D.C. (2019). Proximity labeling of protein complexes and cell-type-specific organellar proteomes in Arabidopsis enabled by TurboID. Elife *8*. 10.7554/eLife.47864.
39. Tang, Y., Huang, A., and Gu, Y. (2020). Global profiling of plant nuclear membrane proteome in Arabidopsis. Nat Plants *6*, 838-847. 10.1038/s41477-020-0700-9.
40. Qin, W., Cho, K.F., Cavanagh, P.E., and Ting, A.Y. (2021). Deciphering molecular interactions by proximity labeling. Nat Methods *18*, 133-143. 10.1038/s41592-020-01010-5.
41. Kraus, M., Pleskot, R., and Van Damme, D. (2024). Structural and evolutionary aspects of plant endocytosis. Annu Rev Plant Biol *75*, 521-550. 10.1146/annurev-arplant-070122-023455.
42. Bhave, N.S., Veley, K.M., Nadeau, J.A., Lucas, J.R., Bhave, S.L., and Sack, F.D. (2009). TOO MANY MOUTHS promotes cell fate progression in stomatal development of Arabidopsis stems. Planta *229*, 357-367. 10.1007/s00425-008-0835-9.
43. Woodward, C., Bemis, S.M., Hill, E.J., Sawa, S., Koshiba, T., and Torii, K.U. (2005). Interaction of auxin and ERECTA in elaborating Arabidopsis inflorescence architecture revealed by the activation tagging of a new member of the YUCCA family putative flavin monooxygenases. Plant Physiol *139*, 192-203. 10.1104/pp.105.063495.
44. Chen, M.K., Wilson, R.L., Palme, K., Ditengou, F.A., and Shpak, E.D. (2013). ERECTA family genes regulate auxin transport in the shoot apical meristem and forming leaf primordia. Plant Physiol *162*, 1978-1991. 10.1104/pp.113.218198.
45. Bergmann, D.C., Lukowitz, W., and Somerville, C.R. (2004). Stomatal development and pattern controlled by a MAPKK kinase. Science *304*, 1494-1497. 10.1126/science.1096014.
46. Herrmann, A., and Torii, K.U. (2021). Shouting out loud: signaling modules in the regulation of stomatal development. Plant Physiol *185*, 765-780. 10.1093/plphys/kiaa061.
47. Chen, L., Cochran, A.M., Waite, J.M., Shirasu, K., Bemis, S.M., and Torii, K.U. (2023). Direct attenuation of Arabidopsis ERECTA signalling by a pair of U-box E3 ligases. Nat Plants *9*, 112-127. 10.1038/s41477-022-01303-x.
48. Yang, X., Wen, Z., Zhang, D., Li, Z., Li, D., Nagalakshmi, U., Dinesh-Kumar, S.P., and Zhang, Y. (2021). Proximity labeling: an emerging tool for probing in planta molecular interactions. Plant Commun *2*, 100137. 10.1016/j.xplc.2020.100137.
49. Xu, S.L., Shrestha, R., Karunadasa, S.S., and Xie, P.Q. (2023). Proximity Labeling in Plants. Annu Rev Plant Biol *74*, 285-312. 10.1146/annurev-arplant-070522-052132.

1021 50. Qian, P., Song, W., Yokoo, T., Minobe, A., Wang, G., Ishida, T., Sawa, S., Chai, J., and
1022 Kakimoto, T. (2018). The CLE9/10 secretory peptide regulates stomatal and vascular
1023 development through distinct receptors. Nat Plants *4*, 1071-1081. 10.1038/s41477-018-
1024 0317-4.
1025 51. Dai, N., Wang, W., Patterson, S.E., and Bleecker, A.B. (2013). The TMK subfamily of
1026 receptor-like kinases in Arabidopsis display an essential role in growth and a reduced
1027 sensitivity to auxin. PLoS One *8*, e60990. 10.1371/journal.pone.0060990.
1028 52. Guo, H., Li, L., Ye, H., Yu, X., Algreen, A., and Yin, Y. (2009). Three related receptor-like
1029 kinases are required for optimal cell elongation in Arabidopsis thaliana. Proc Natl Acad
1030 Sci U S A *106*, 7648-7653. 10.1073/pnas.0812346106.
1031 53. Le, M.H., Cao, Y., Zhang, X.C., and Stacey, G. (2014). LIK1, a CERK1-interacting kinase,
1032 regulates plant immune responses in Arabidopsis. PLoS One *9*, e102245.
1033 10.1371/journal.pone.0102245.
1034 54. Wallner, E.S., Mair, A., Handler, D., McWhite, C., Xu, S.L., Dolan, L., and Bergmann, D.C.
1035 (2024). Spatially resolved proteomics of the Arabidopsis stomatal lineage identifies
1036 polarity complexes for cell divisions and stomatal pores. Dev Cell *59*, 1096-1109 e1095.
1037 10.1016/j.devcel.2024.03.001.
1038 55. Kinoshita, T., Doi, M., Suetsugu, N., Kagawa, T., Wada, M., and Shimazaki, K. (2001).
1039 Phot1 and phot2 mediate blue light regulation of stomatal opening. Nature *414*, 656-660.
1040 10.1038/414656a.
1041 56. Ho, C.M., Paciorek, T., Abrash, E., and Bergmann, D.C. (2016). Modulators of stomatal
1042 lineage signal transduction alter membrane contact sites and reveal specialization among
1043 ERECTA kinases. Dev Cell *38*, 345-357. 10.1016/j.devcel.2016.07.016.
1044 57. Xue, X., Wang, L., Huang, A., Liu, Z., Guo, X., Sang, Y., Zhu, J.K., Xue, H., and Dong, J.
1045 (2024). Membrane-associated NRPM proteins are novel suppressors of stomatal
1046 production in Arabidopsis. Curr Biol *34*, 881-894 e887. 10.1016/j.cub.2024.01.052.
1047 58. Szklarczyk, D., Kirsch, R., Koutrouli, M., Nastou, K., Mehryary, F., Hachilif, R., Gable, A.L.,
1048 Fang, T., Doncheva, N.T., Pyysalo, S., et al. (2023). The STRING database in 2023:
1049 protein-protein association networks and functional enrichment analyses for any
1050 sequenced genome of interest. Nucleic Acids Res *51*, D638-d646. 10.1093/nar/gkac1000.
1051 59. Fujimoto, M., Ebine, K., Nishimura, K., Tsutsumi, N., and Ueda, T. (2020). Longin R-
1052 SNARE is retrieved from the plasma membrane by ANTH domain-containing proteins in
1053 Arabidopsis. Proc Natl Acad Sci U S A *117*, 25150-25158. 10.1073/pnas.2011152117.
1054 60. Kim, E.J., Zhang, C., Guo, B., Eekhout, T., Houbaert, A., Wendrich, J.R., Vandamme, N.,
1055 Tiwari, M., Simon--Vezo, C., Vanhoutte, I., et al. (2023). Cell type-specific attenuation of
1056 brassinosteroid signaling precedes stomatal asymmetric cell division. Proc Natl Acad Sci
1057 U S A *120*. ARTN e230375812010.1073/pnas.2303758120.
1058 61. Minamino, N., Fujii, H., Murata, H., Hachinoda, S., Kondo, Y., Hotta, K., and Ueda, T.
1059 (2023). Analysis of plant-specific ANTH domain-containing protein in Marchantia
1060 polymorpha. Plant Cell Physiol *64*, 1331-1342. 10.1093/pcp/pcad118.
1061 62. Takahashi, H., Uematsu, A., Yamanaka, S., Imamura, M., Nakajima, T., Doi, K., Yasuoka,
1062 S., Takahashi, C., Takeda, H., and Sawasaki, T. (2016). Establishment of a Wheat Cell-
1063 Free Synthesized Protein Array Containing 250 Human and Mouse E3 Ubiquitin Ligases
1064 to Identify Novel Interaction between E3 Ligases and Substrate Proteins. Plos One *11*.
1065 ARTN e0156718 10.1371/journal.pone.0156718.
1066 63. Geldner, N., Anders, N., Wolters, H., Keicher, J., Kornberger, W., Muller, P., Delbarre, A.,
1067 Ueda, T., Nakano, A., and Jurgens, G. (2003). The Arabidopsis GNOM ARF-GEF
1068 mediates endosomal recycling, auxin transport, and auxin-dependent plant growth. Cell
1069 *112*, 219-230. 10.1016/s0092-8674(03)00003-5.
1070 64. Chen, Y., and Weckwerth, W. (2020). Mass spectrometry untangles plant membrane
1071 protein signaling networks. Trends Plant Sci *25*, 930-944. 10.1016/j.tplants.2020.03.013.

1072 65. Cuadrado, A.F., and Van Damme, D. (2024). Unlocking protein-protein interactions in
1073 plants: a comprehensive review of established and emerging techniques. J Exp Bot *75*,
1074 5220-5236. 10.1093/jxb/erae088.
1075 66. Jiang, H., Chen, Y., Liu, Y., Shang, J., Sun, X., and Du, J. (2022). Multifaceted roles of
1076 the ERECTA family in plant organ morphogenesis. J Exp Bot *73*, 7208-7218.
1077 10.1093/jxb/erac353.
1078 67. Feng, Y., Hiwatashi, T., Minamino, N., Ebine, K., and Ueda, T. (2022). Membrane
1079 trafficking functions of the ANTH/ENTH/VHS domain-containing proteins in plants. FEBS
1080 Lett *596*, 2256-2268. 10.1002/1873-3468.14368.
1081 68. Muro, K., Matsuura-Tokita, K., Tsukamoto, R., Kanaoka, M.M., Ebine, K., Higashiyama,
1082 T., Nakano, A., and Ueda, T. (2018). ANTH domain-containing proteins are required for
1083 the pollen tube plasma membrane integrity via recycling ANXUR kinases. Commun Biol
1084 *1*, 152. 10.1038/s42003-018-0158-8.
1085 69. Teixeira, R.T., Marchese, D., Duckney, P.J., Dias, F.V., Carapeto, A.P., Louro, M., Silva,
1086 M.S., Cordeiro, C., Rodrigues, M.S., and Malhó, R. (2025). Functional characterization
1087 reveals the importance of Arabidopsis and in clathrin mediated endocytosis and wall
1088 structure in apical growing cells. New Phytologist *245*, 1056-1071. 10.1111/nph.20282.
1089 70. Nguyen, H.H., Lee, M.H., Song, K., Ahn, G., Lee, J., and Hwang, I. (2018). The A/ENTH
1090 domain-containing protein AtECA4 Is an adaptor protein involved in cargo recycling from
1091 the trans-Golgi Network/Early Endosome to the plasma membrane. Mol Plant *11*, 568-
1092 583. 10.1016/j.molp.2018.01.001.
1093 71. Lampard, G.R., Macalister, C.A., and Bergmann, D.C. (2008). Arabidopsis stomatal
1094 initiation is controlled by MAPK-mediated regulation of the bHLH SPEECHLESS. Science
1095 *322*, 1113-1116. 10.1126/science.1162263.
1096 72. Putarjunan, A., Ruble, J., Srivastava, A., Zhao, C., Rychel, A.L., Hofstetter, A.K., Tang, X.,
1097 Zhu, J.K., Tama, F., Zheng, N., and Torii, K.U. (2019). Bipartite anchoring of SCREAM
1098 enforces stomatal initiation by coupling MAP kinases to SPEECHLESS. Nat Plants *5*, 742-
1099 754. 10.1038/s41477-019-0440-x.
1100 73. Fung, H.F., Amador, G.O., Dale, R., Gong, Y., Vollbrecht, M., Erberich, J.M., Mair, A., and
1101 Bergmann, D.C. (2025). Multi-scale dynamics influence the division potential of stomatal
1102 lineage ground cells in Arabidopsis. Nat Commun *16*, 2612. 10.1038/s41467-025-57730-
1103 9.
1104 74. Qi, X., Han, S.K., Dang, J.H., Garrick, J.M., Ito, M., Hofstetter, A.K., and Torii, K.U. (2017).
1105 Autocrine regulation of stomatal differentiation potential by EPF1 and ERECTA-LIKE1
1106 ligand-receptor signaling. Elife *6*. 10.7554/eLife.24102.
1107 75. Zeng, S.M., Lo, E.K.W., Hazelton, B.J., Morales, M.F., and Torii, K.U. (2020). Effective
1108 range of non-cell autonomous activator and inhibitor peptides specifying plant stomatal
1109 patterning. Development *147*. 10.1242/dev.192237.
1110 76. Leng, Y.J., Yao, Y.S., Yang, K.Z., Wu, P.X., Xia, Y.X., Zuo, C.R., Luo, J.H., Wang, P., Liu,
1111 Y.Y., Zhang, X.Q., et al. (2022). Arabidopsis ERdj3B coordinates with ERECTA-family
1112 receptor kinases to regulate ovule development and the heat stress response. Plant Cell
1113 *34*, 3665-3684. 10.1093/plcell/koac226.
1114 77. Yang, K.Z., Zuo, C.R., Leng, Y.J., Yue, J.L., Liu, H.C., Fan, Z.B., Xue, X.Y., Dong, J.,
1115 Chen, L.Q., and Le, J. (2022). The functional specificity of ERECTA-family receptors in
1116 Arabidopsis stomatal development is ensured by molecular chaperones in the
1117 endoplasmic reticulum. Development *149*. 10.1242/dev.200892.
1118 78. Martins, S., Dohmann, E.M.N., Cayrel, A., Johnson, A., Fischer, W., Pojer, F., Satiat-
1119 Jeunemaître, B., Jaillais, Y., Chory, J., Geldner, N., and Vert, G. (2015). Internalization
1120 and vacuolar targeting of the brassinosteroid hormone receptor BRI1 are regulated by
1121 ubiquitination. Nature Communications *6*. ARTN 615110.1038/ncomms7151.

1122 79. Chen, L., Vu, M.H., Cochran, A.M., Ying, C.F., and Torii, K.U. (2025). Ligand-induced
1123 ubiquitination regulates endocytosis and homeostasis of the ERECTA receptor kinase for
1124 stomatal development. bioRxiv, 2025.2006. 2029.662054.
1125 80. Ebine, K., Fujimoto, M., Okatani, Y., Nishiyama, T., Goh, T., Ito, E., Dainobu, T., Nishitani,
1126 A., Uemura, T., Sato, M.H., et al. (2011). A membrane trafficking pathway regulated by
1127 the plant-specific RAB GTPase ARA6. Nat Cell Biol *13*, 853-859. 10.1038/ncb2270.
1128 81. Nakagawa, T., Nakamura, S., Tanaka, K., Kawamukai, M., Suzuki, T., Nakamura, K.,
1129 Kimura, T., and Ishiguro, S. (2008). Development of R4 gateway binary vectors (R4pGWB)
1130 enabling high-throughput promoter swapping for plant research. Biosci Biotechnol
1131 Biochem *72*, 624-629. 10.1271/bbb.70678.
1132 82. Ogawa, S., Miyamoto, K., Nemoto, K., Sawasaki, T., Yamane, H., Nojiri, H., and Okada,
1133 K. (2017). OsMYC2, an essential factor for JA-inductive sakuranetin production in rice,
1134 interacts with MYC2-like proteins that enhance its transactivation ability. Sci Rep *7*, 40175.
1135 10.1038/srep40175.
1136 83. Yano, T., Takeda, H., Uematsu, A., Yamanaka, S., Nomura, S., Nemoto, K., Iwasaki, T.,
1137 Takahashi, H., and Sawasaki, T. (2016). AGIA Tag System Based on a High Affinity Rabbit
1138 Monoclonal Antibody against Human Dopamine Receptor D1 for Protein Analysis. PLoS
1139 One *11*, e0156716. 10.1371/journal.pone.0156716.
1140 84. Zhang, X., Henriques, R., Lin, S.S., Niu, Q.W., and Chua, N.H. (2006). Agrobacterium-
1141 mediated transformation of Arabidopsis thaliana using the floral dip method. Nat Protoc *1*,
1142 641-646. 10.1038/nprot.2006.97.
1143 85. Shannon, P., Markiel, A., Ozier, O., Baliga, N.S., Wang, J.T., Ramage, D., Amin, N.,
1144 Schwikowski, B., and Ideker, T. (2003). Cytoscape: a software environment for integrated
1145 models of biomolecular interaction networks. Genome Res *13*, 2498-2504.
1146 10.1101/gr.1239303.
1147 86. Yoo, S.D., Cho, Y.H., and Sheen, J. (2007). Arabidopsis mesophyll protoplasts: a versatile
1148 cell system for transient gene expression analysis. Nat Protoc *2*, 1565-1572.
1149 10.1038/nprot.2007.199.
1150 87. Avila, J.R., Lee, J.S., and Torii, K.U. (2015). Co-Immunoprecipitation of Membrane-Bound
1151 Receptors. Arabidopsis Book *13*, e0180. 10.1199/tab.0180.
1152 88. Sawasaki, T., Kamura, N., Matsunaga, S., Saeki, M., Tsuchimochi, M., Morishita, R., and
1153 Endo, Y. (2008). Arabidopsis HY5 protein functions as a DNA-binding tag for purification
1154 and functional immobilization of proteins on agarose/DNA microplate. FEBS Lett *582*, 221-
1155 228. 10.1016/j.febslet.2007.12.004.
1156 89. Nemoto, K., Kagawa, M., Nozawa, A., Hasegawa, Y., Hayashi, M., Imai, K., Tomii, K., and
1157 Sawasaki, T. (2018). Identification of new abscisic acid receptor agonists using a wheat
1158 cell-free based drug screening system. Sci Rep *8*, 4268. 10.1038/s41598-018-22538-9.
1159 90. Lu, P., Vogel, C., Wang, R., Yao, X., and Marcotte, E.M. (2007). Absolute protein
1160 expression profiling estimates the relative contributions of transcriptional and translational
1161 regulation. Nat Biotechnol *25*, 117-124. 10.1038/nbt1270.
1162 91. Lee, C., Cox, R.M., Papoulas, O., Horani, A., Drew, K., Devitt, C.C., Brody, S.L., Marcotte,
1163 E.M., and Wallingford, J.B. (2020). Functional partitioning of a liquid-like organelle during
1164 assembly of axonemal dyneins. Elife *9*. 10.7554/eLife.58662.
1165

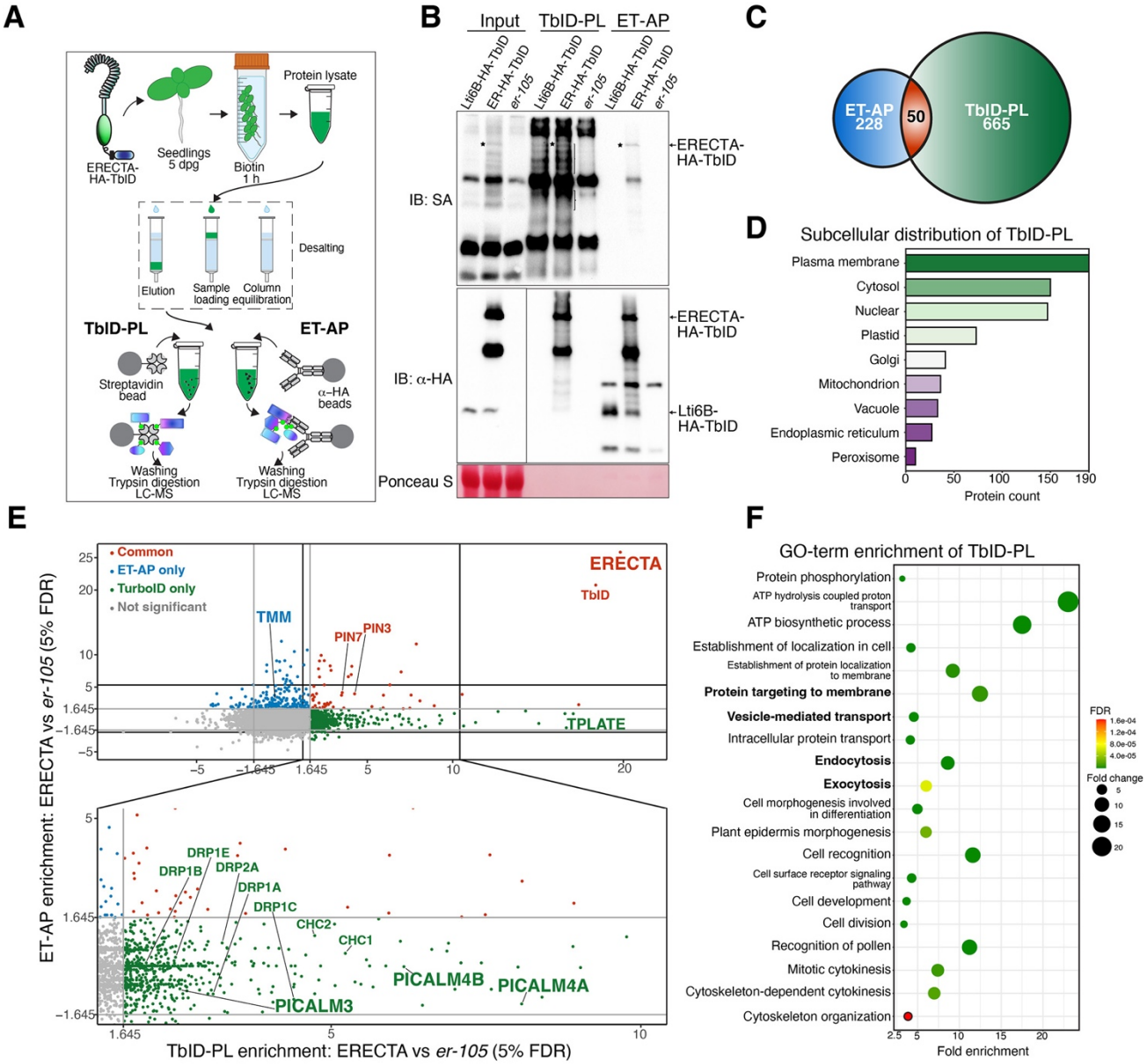

Figure 1. Comparative proteomic profiling of ERECTA-associated proteins.
(A) Schematic representation of the experimental workflow for profiling ERECTA-associated proteins using TbID-PL and ET-AP. Parallel enrichments of biotinylated proteins and HA-tagged protein complexes were subjected to mass spectrometry analysis.
(B) Immunoblot validation of ERECTA and its associated proteins. Streptavidin-HRP (SA-HRP) (top) confirms successful biotinylation of proximal proteins via TbID-PL. α-HA immunoblot (middle) verifies the expression and enrichment of ERECTA-HA-TbID. Ponceau S staining (bottom) indicates loading control.
(C) Venn diagram of identified proteins reveals 665 unique to TbID-PL, 228 unique to ET-AP, and 50 shared proteins.
(D) Subcellular localization of TbID-PL enriched proteins, showing enrichment at the plasma membrane and cytosol, with additional representation in endomembrane compartments.

1181 (E) Scatterplot comparing protein enrichment between TbID-PL and ET-AP. Notable components
1182 of clathrin-mediated endocytosis (CME), such as PICALMs, DRPs, and TPLATE complex
1183 members, are preferentially captured by TbID-PL. In contrast, stable receptor partners like TMM
1184 are enriched via ET-AP. Some auxin transporters (PIN3, PIN7) are recovered in both methods.
1185 (F) GO-term enrichment of TbID-PL-identified proteins reveals overrepresentation of membrane
1186 trafficking, endocytosis, protein localization, and epidermal development terms. Circle size
1187 represents fold enrichment; color indicates false discovery rate (FDR) values.
1188
1189

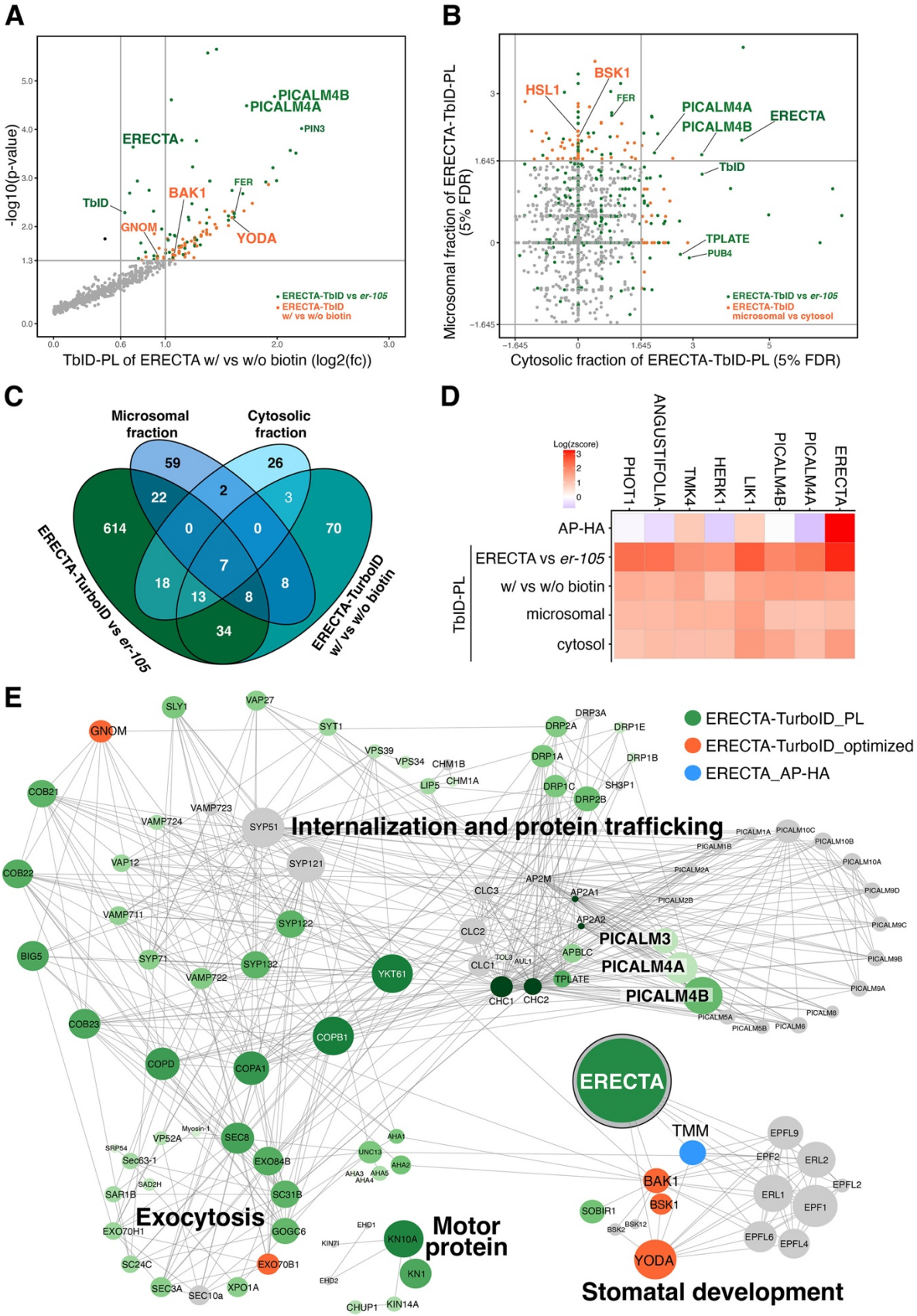
A
-log10(p-value)
TbID-PL of ERECTA w/ vs w/o biotin (log2(fc))
PICALM4B
PICALM4A
PIN3
ERECTA
FER
BAK1
TbID
GNOM
YODA
ERECTA-TbID vs er-105
ERECTA-TbID w/ vs w/o biotin
B
Microsomal fraction of ERECTA-TbID-PL (5% FDR)
Cytosolic fraction of ERECTA-TbID-PL (5% FDR)
BSK1
HSL1
FER
PICALM4A
PICALM4B
ERECTA
TbID
TPLATE
PUB4
ERECTA-TbID vs er-105
ERECTA-TbID microsomal vs cytosol
C
Microsomal fraction
Cytosolic fraction
ERECTA-TurboID vs er-105
ERECTA-TurboID w/ vs w/o biotin
D
Log(zscore)
PHOT1
ANGUSTIFOLIA
TMK4
HERK1
LIK1
PICALM4B
PICALM4A
ERECTA
AP-HA
TbID-PL
ERECTA vs er-105
w/ vs w/o biotin
microsomal
cytosol
E
ERECTA-TurboID_PL
ERECTA-TurboID_optimized
ERECTA_AP-HA
Internalization and protein trafficking
PICALM3
PICALM4A
PICALM4B
ERECTA
TMM
BAK1
BSK1
YODA
Exocytosis
Motor protein
Stomatal development

1190

1191
1192 **Figure 2. Optimized TbID-PL enhances detection of ERECTA-associated signaling**
1193 **components and compartment-specific proteomes.**
1194 (A) Scatterplot showing differential enrichment of biotinylated proteins in ERECTA-TbID-PL with
1195 biotin versus without biotin treatments. Several known ERECTA signaling components, including
1196 BAK1, YODA (MAPKKK4) are identified (orange) alongside clathrin-mediated endocytosis
1197 proteins (e.g., PICALM4A, PICALM4B) identified (green) in figure 1.
1198 (B) Scatterplot comparing enrichment between microsomal and cytosolic fractionation in TbID-PL
1199 proteomes. Membrane-attached receptor-like cytoplasmic kinase BSK1 is predominantly
1200 enriched in the microsomal fraction, while CME components (e.g., PICALM4A, 4B) and ERECTA
1201 are detected in both fractions.
1202 (C) Venn diagram showing overlap among TbID-PL datasets derived from comparisons of
1203 ERECTA-HA-TbID vs *er-105*, +biotin vs -biotin, and microsomal vs cytosolic fractions. Seven
1204 candidates are consistently detected across all comparisons.
1205 (D) Heatmap showing normalized enrichment (log2 z-scores) of the top 7 consistently identified
1206 ERECTA-proximal proteins across four TbID-PL conditions. These include ERECTA itself,
1207 PICALM4A/B, and kinases implicated in receptor signaling (LIK1, HERK1, TMK4), as well as
1208 ANGUSTIFOLIA and PHOT1.
1209 (E) STRING network analysis of ERECTA-associated proteins identified by TbID-PL (green),
1210 optimized TbID-PL (orange), or ET-AP (blue). Proteins are clustered into major functional
1211 categories: internalization/protein trafficking, exocytosis, motor proteins, and stomatal
1212 development. ERECTA, CME components (PICALMs, TPLATE, DRPs), and signaling partners
1213 (e.g., BAK1, YODA, TMM) are highlighted. Node size reflects interaction confidence.
1214
1215

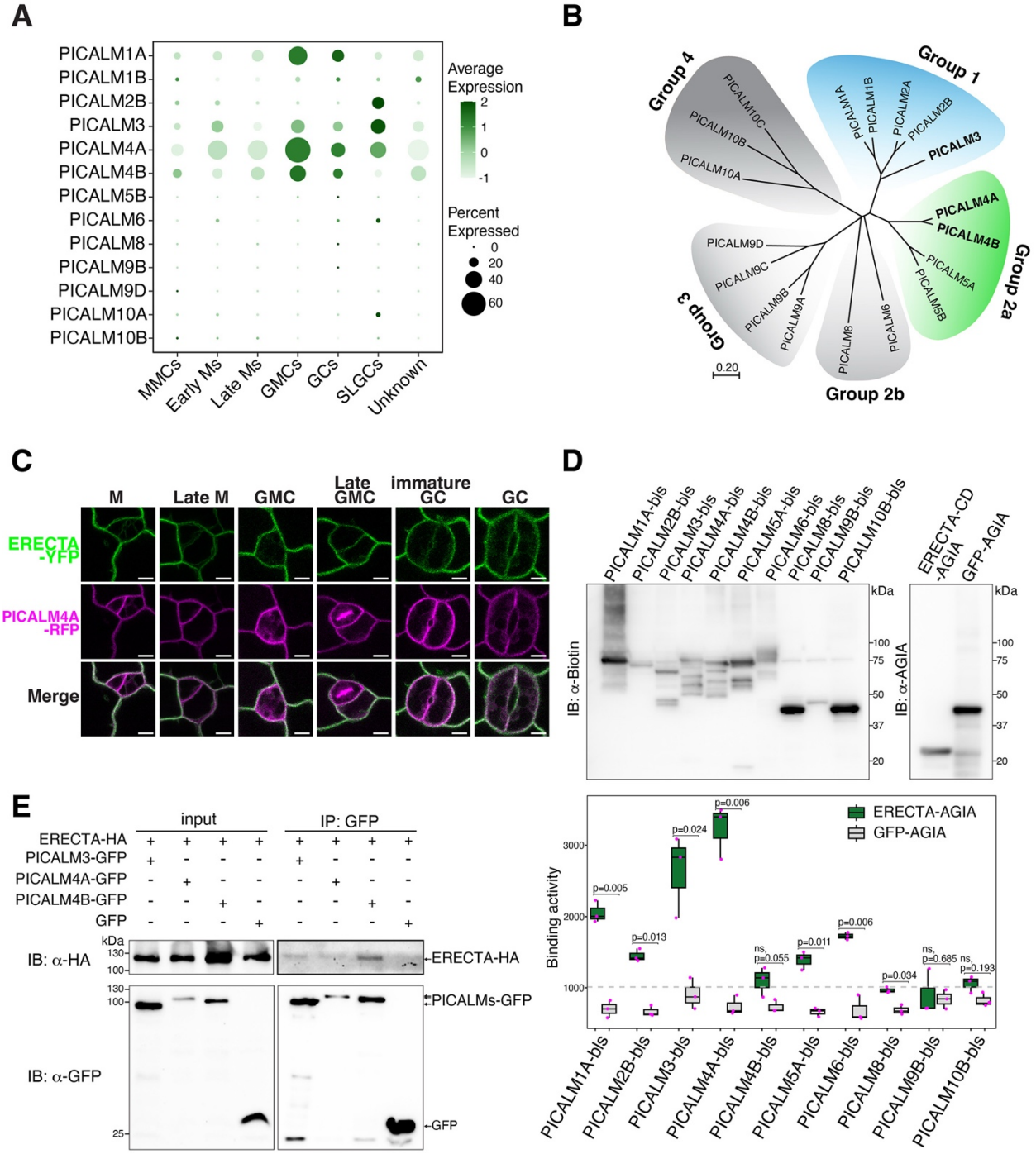

Figure 3. ERECTA selectively interacts with PICALM family of clathrin-mediated endocytosis (CME) components.

(A) Dot plot showing transcriptional expression of Arabidopsis PICALM family genes across stomatal lineage cell types from re-analyzed single-cell RNA-seq data. PICALM1, PICALM3, PICALM4A, and PICALM4B are present across different stages of stomatal lineage cells. PICALM1, PICALM4A, and PICALM4B are highly enriched in guard mother cell (GMC), guard cell (GC) stages, while PICALM2B and PICALM3 are highly enriched in stomatal lineage ground

cells (SLGCs). The distinct expression of PICALMs suggest their potential roles in different stage of stomatal development. Dot size indicates proportion of expressing cells; dot color reflects expression levels.

(B) Phylogenetic tree of Arabidopsis PICALM family members. PICALM3 (Group 1, blue) and PICALM4A/B (Group 2a, green) cluster into distinct clades with high proximity to ERECTA based on TbID-PL. The phylogenetic tree illustrates evolutionary relationships and potential functional specialization within PICALM family.

(C) Confocal microscopy showing subcellular colocalization of endogenous promoters-driven ERECTA-YFP and PICALM4A-RFP in cotyledon epidermal cells at multiple stomatal lineage stages. M, meristemoid; GMC, guard mother cell; GC, guard cell. Scale bars, 10 μm. ERECTA-YFP colocalizes with PICALM4A-RFP at the plasma membrane in stomatal lineage cells, except at cell plates for dividing cells.

(D) *In vitro* protein-protein interacting assay between ERECTA and PICALM family proteins. ERECTA cytoplasmic domain and PICALMs were *in vitro* translated for the AlphaScreen assay. Quantification of normalized binding activity (right) confirms the preferential binding for PICALM3, PICALM4A, and PICALM1A. Boxplots represent mean with SD from three biological replicates and significance was assessed by unpaired t-test.

(E) Co-immunoprecipitation assays validating interactions between ERECTA and PICALM proteins transiently co-expressed in Arabidopsis protoplasts. Immunoblot analysis confirmed *in-vivo* binding of ERECTA-HA to PICALM3-GFP, PICALM4A-GFP, and PICALM4B-GFP, as shown in the red-boxed lanes.

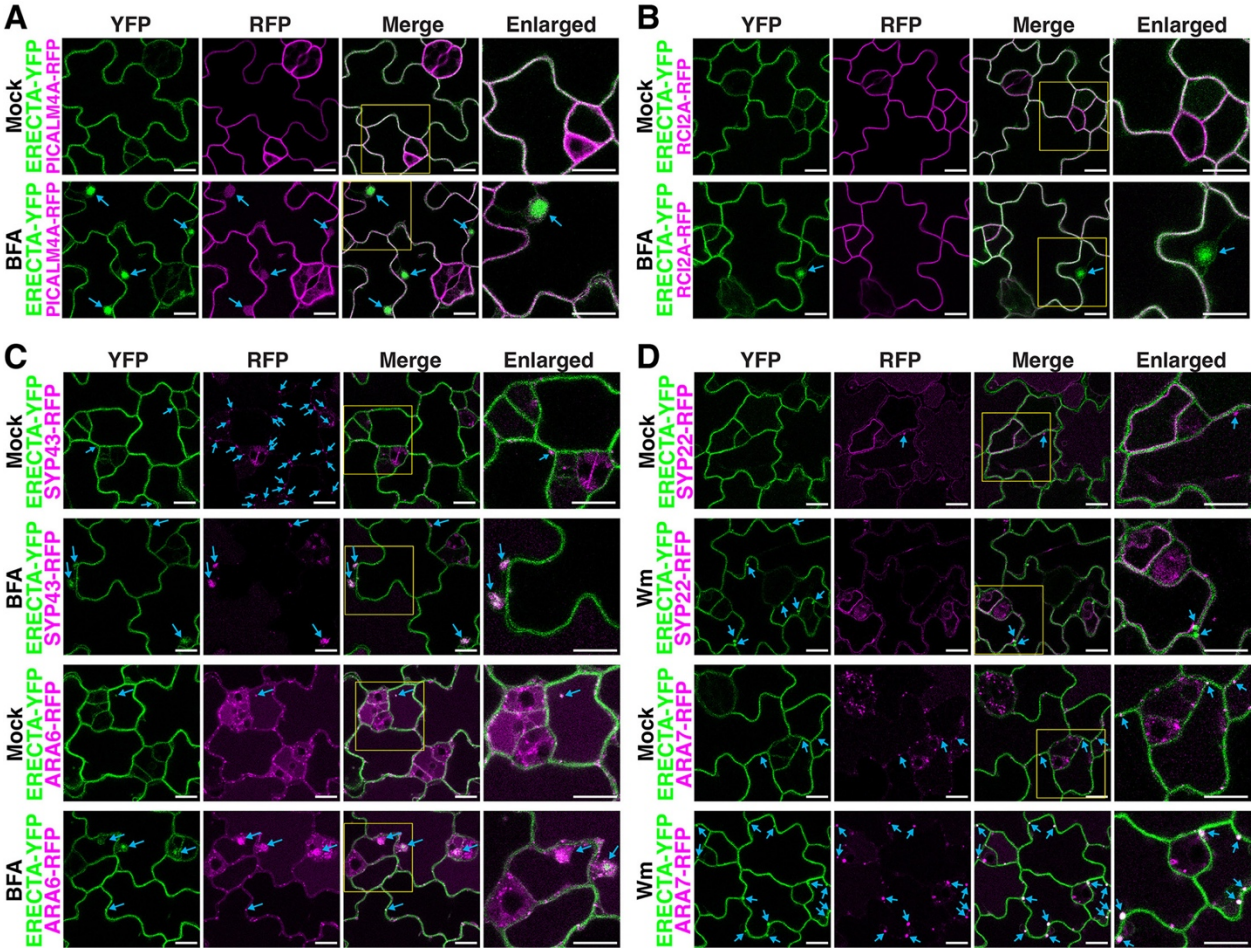

Figure 4. ERECTA-YFP co-localizes with PICALM4A and endosomal markers in stomatal-lineage cells.

(A) Confocal microscopy showing colocalization of ERECTA-YFP with PICALM4A-RFP under mock and BFA-treated conditions. In untreated cells, both proteins localize to the plasma membrane. Brefeldin A (BFA) treatment results in BFA-induced endosomal compartments, where PICALM4A-RFP encapsulates and colocalizes with ERECTA-YFP (arrowheads).

(B) Confocal microscopy showing that ERECTA-YFP does not colocalize with the plasma membrane marker RCI2A-mCherry in BFA bodies. Under BFA treatment, ERECTA-YFP is redistributed to endosomal compartments (arrowheads), while RCI2A-mCherry remains at the plasma membrane, indicating selective internalization of ERECTA.

(C) Confocal microscopy imaging of ERECTA-YFP with the trans-Golgi network (TGN) marker SYP43-RFP (top) and the plasma membrane/early endosome marker ARA6-RFP (bottom). Under mock conditions, ERECTA-YFP localizes to the plasma membrane and partially colocalizes with SYP43 and ARA6 (arrowheads). Following BFA treatment, ERECTA-YFP colocalized with both SYP43-RFP and ARA6-RFP in BFA-induced endosomal compartments, confirming its trafficking through the TGN and early endosomes.

(D) Confocal microscopy showing colocalization of ERECTA-YFP with the late endosome marker ARA7-RFP and the vacuolar membrane marker SYP22-RFP. Under mock conditions, limited colocalization is observed. Upon wortmannin treatment, ERECTA-YFP co-localizes with ARA7-RFP in these enlarged endosomes, indicating ERECTA's progression toward late endosome and vacuoles.

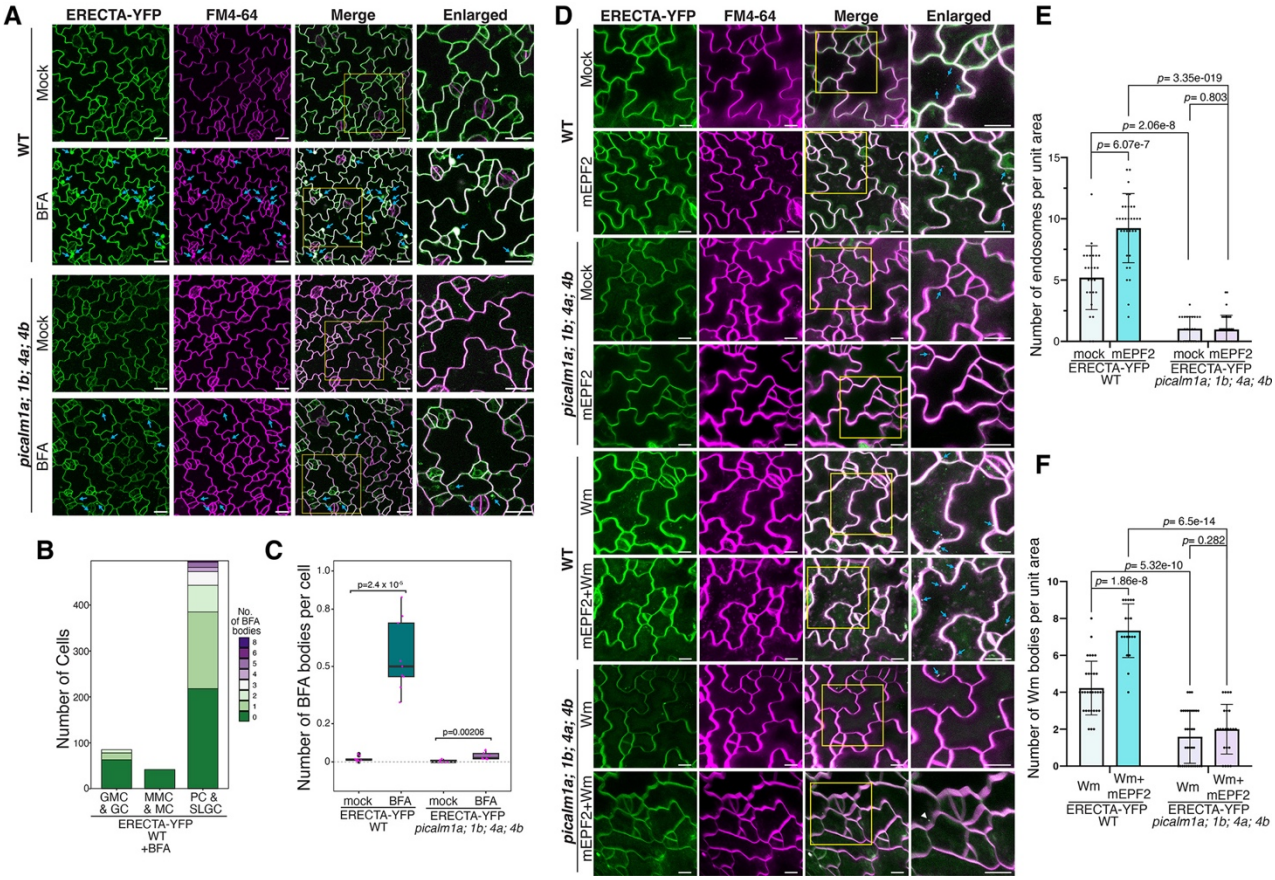

Figure 5. PICALM proteins regulate ERECTA internalization.

(A) Confocal images of ERECTA-YFP internalization in WT and *picalm1a;1b;4a;4b* mutants under mock and BFA treatment. In WT, BFA induces the formation of ERECTA-YFP–positive endosomal compartments (BFA bodies, arrowheads). Whereas the number of BFA body is markedly reduced in the *picalm1a;1b;4a;4b* mutant, indicating impaired endocytic recycling.

(B) Quantification of the number of cells with BFA bodies across stomatal lineage stages in WT. ERECTA-YFP endocytic activity is enriched in pavement cells (PCs) and stomatal lineage ground cells (SLGCs).

(C) Box plot quantifying the number of BFA bodies per cell under mock and BFA treatments in WT and *picalm1a;1b;4a;4b* mutants. WT shows a significant increase in BFA bodies upon treatment, while *picalm1a;1b;4a;4b* mutant exhibits no significant response.

(D) Confocal microscopy images showing ERECTA-YFP internalization in response to mEPF2 peptide, wortmannin, or their combination in WT and *picalm1a;1b;4a;4b* mutants. In WT, mEPF2 triggers endocytic accumulation of ERECTA-YFP that overlaps with FM4-64, and Wm enlarges late endosomes containing ERECTA-YFP. These responses are strongly reduced in the *picalm1a;1b;4a;4b* mutant (arrowheads).

(E) Quantification of mEPF2-induced ERECTA-YFP puncta in WT and *picalm1a;1b;4a;4b* mutants shows impaired ligand-triggered ERECTA endocytosis in the mutant.

(F) Quantification of ERECTA-YFP positive Wm bodies per cell in WT and *picalm1a;1b;4a;4b* mutant. Wm-induced accumulation is significantly reduced in the mutant, indicating defective trafficking to late endosomes.

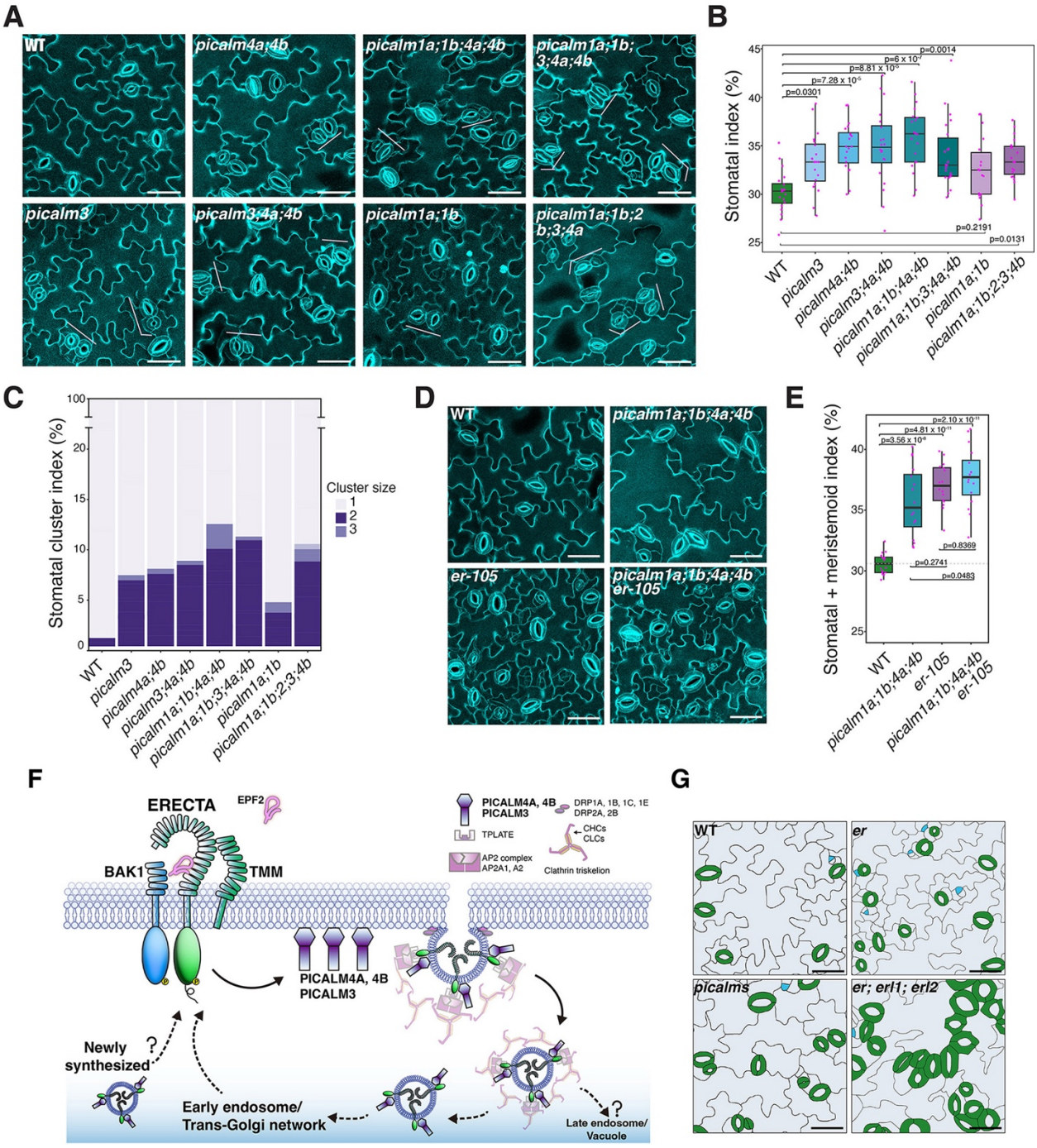

Figure 6. *PICALMs* are required for proper stomatal patterning

(A) Confocal images of abaxial epidermis from wild-type (WT) and various *picalm* single, double, and higher-order mutants. WT plants exhibit normal stomatal development, whereas *picalm* mutants exhibit increased stomatal index with varying degrees of stomatal clustering. Scale bars, 40 µm.

(B) Quantification of stomatal index in WT and *picalm* mutants. Box plots show a significant increase in stomatal index in *picalm* mutants compared to WT. Statistical analysis was determined using one-way ANOVA followed by Tukey's HSD test.

1310 (C) Stomatal cluster index analysis in WT and *picalm* mutants. Stomatal clusters are categorized
1311 by size (e.g., two, three, or four stomata per cluster), highlighting a dramatic rise in clustering
1312 frequency in higher-order *picalm* mutants.
1313 (D) Confocal images of abaxial epidermis from WT, *er-105*, *picalm1a;1b;4a;4b*, and the quintuple
1314 mutant *picalm1a;1b;4a;4b;er-105*. The quintuple mutant shows similar stomatal numbering and
1315 clustering to *er-105*. Scale bars, 40 μm.
1316 (E) Quantification of combined stomatal and meristemoid index. The *picalm1a;1b;4a;4b;er-105*
1317 quintuple mutant exhibits values comparable to *er-105*, indicating that PICALMs act in the same
1318 genetic pathway as ERECTA.
1319 (F) Proposed model of the ERECTA receptor internalization facilitated by PICALM proteins.
1320 ERECTA is internalized through CME involving adaptor proteins such as PICALM3, PICALM4A,
1321 and PICALM4B, along with the AP2 complex and TPLATE. Internalized receptors are sorted via
1322 early endosomes or the trans-Golgi network (TGN) for recycling, or trafficked to vacuoles for
1323 degradation. In *picalm* mutants, defective CME impairs receptor pool balance, disrupting stomatal
1324 patterning. The secretion of newly synthesized ERECTA and trafficking to late
1325 endosomes/vacuoles remain unresolved in *picalm* mutants.
1326 (G) Representative images comparing stomatal patterning in WT, *picalms, er,* and *er; erl1; erl2*
1327 mutants. *picalm* mutants phenocopy *er* family mutants, displaying increased stomatal number and
1328 clustering, supporting a functional link between CME regulation and ERECTA-mediated signaling.
1329